Regional and Diurnal Variability of the Vertical Structure of Precipitation Systems in Africa Based on Spaceborne Radar Data

BART GEERTS AND TEFERI DEJENE

Department of Atmospheric Science, University of Wyoming, Laramie, Wyoming

(Manuscript received 13 April 2004, in final form 2 September 2004)

ABSTRACT

The Tropical Rainfall Measuring Mission (TRMM) 2A25 radar reflectivity profiles and derived surface rain rates are used to describe the vertical structure of precipitation systems in Africa. Five years of data are used in both the boreal and austral summer rainy seasons. A number of climate regions are isolated and compared. To place the composite reflectivity profiles in context, they are contrasted against TRMM 2A25 observations over the Amazon.

In all of tropical Africa, precipitation systems tend to be deeper and more intense than in the Amazon, and shallow warm-rain events are less common. In all African regions, but especially in the Sahel and northern Savanna, storms are characterized by high echo tops, high hydrometeor loading aloft, little indication of a radar brightband maximum at the freezing level, and evidence for low-level evaporation.

Storms in Africa are generally most common, and deepest, in the late afternoon, and weaker shallow systems are relatively more common around noon. The diurnal modulation is regionally variable. The amplitude of the diurnal cycle of the mean echo top height decreases from the arid margins of the zenithal rain region toward the equatorial region, and is smallest in the Amazon. A secondary predawn (0000–0600 LT) maximum occurs in the Congo, in terms of rainfall frequency, rainfall intensity, and echo tops. The storm intensity indicators generally peak a few hours later in the Sahel and northern Savanna than in other regions in Africa.

The difference between all African regions and the Amazon, and the relatively smaller differences between regions in Africa, can be understood in terms of the climatological humidity, CAPE, and low-level shear values.

1. Introduction

Spaceborne rainfall estimation has evolved dramatically over the last two decades (e.g., Huffman et al. 1997). Spaceborne techniques, usually guided by rain gauge data, have been developed based on IR brightness temperatures (e.g., Vicente et al. 1996), multifrequency passive microwave radiances (e.g., Kummerow and Giglio 1994), or a combination of these two. Obviously IR-based techniques have weaknesses, in particular because the anvil of large convective systems is much larger than the precipitation shafts underneath, and the anvil topography is more uniform. Upwelling microwave radiation, emitted or scattered by hydrometeors at all levels in the precipitation column, is more sensitive to these underlying precipitation shafts.

A new era of spaceborne precipitation research started in late November 1997 with the launch of the Tropical Rainfall Measuring Mission (TRMM) satellite (Kummerow et al. 2000). The TRMM satellite instrument package includes a 13.8-GHz (2.2-cm) radar, the Precipitation Radar (PR; Kummerow et al. 1998). Radar reflectivity data, especially its vertical structure, can be used to improve surface rainfall estimation (e.g., Ferreira et al. 2001). Large differences exist between passive microwave and radar-based rain-rate estimates, mainly on an instantaneous basis, but also cumulatively (Kummerow et al. 2000).

Spaceborne radar data can be used also to characterize the horizontal and vertical structure of precipitation systems. Precipitation Radar reflectivity maps document the horizontal structure of storms and yield information about mesoscale organization, which links to storm longevity (e.g., Heymsfield et al. 2000). Especially intriguing is the PR's ability to describe the vertical structure of storms in detail, on account of the PR's near-vertical incidence. The vertical profile of reflectivity can be used to estimate the profiles of radiative and latent heating (Jensen and Del Genio 2003): as storms develop and decay, they leave behind footprints of condensational heating and evaporative cooling at various levels in the troposphere, and these are an im-

Corresponding author address: Dr. Bart Geerts, Department of Atmospheric Science, University of Wyoming, Laramie, WY 82071.
E-mail: geerts@uwyo.edu

© 2005 American Meteorological Society

portant component in the tropical general circulation (e.g., Mapes and Houze 1993).

This paper focuses on the vertical structure of precipitation systems. Most tropical precipitation systems are deep, but a significant portion of tropical rainfall results from shallow systems with tops near the freezing level (Petty 1999; Johnson et al. 1999; Berg et al. 2002). The fraction of the rainfall from shallow systems, either cumuli congesti or shallow nimbostratus, is poorly understood, and it probably varies significantly regionally and seasonally.

A fundamental distinction exists between convective and stratiform precipitation regions within deep precipitation systems (Houze 1997). In stratiform regions, hydrometeors fall from the upper-cloud layers while they grow, and they produce a distinct reflectivity maximum at the freezing level (FL), known as the bright band (Houze 1993). In essence this bright band is due to the wet coating of melting snowflakes (Battan 1973). In regions of deep convection, a bright band is absent, because the melting of heavily rimed hydrometeors occurs over a deeper layer, and the changes in fall speed are smaller. Also, reflectivity decays more slowly with height above the FL, when compared with that in stratiform regions. The rain type distinction is important because different rain types have different Z–R (reflectivity–rain-rate) relationships (e.g., Steiner and Houze 1997), and different profiles of latent heating. The above-mentioned discrepancy between passive microwave and radar-based rain-rate estimates appears to be related to differences in vertical structure of precipitation systems, specifically their depth and convective/stratiform nature (Masunaga et al. 2002).

The TRMM PR data, in conjunction with passive microwave and lightning data collected aboard the TRMM satellite, have revealed remarkable differences between continental and maritime precipitation systems in the Tropics (e.g., Toracinta et al. 2002; Cecil and Zipser 2002; Nesbitt and Zipser 2003). Maritime systems tend to have less lightning, less ice aloft, more stratiform characteristics, and they are less diurnally modulated, as compared to continental systems. A comparison between two equatorial wet regions, the Congo and the Amazon basins, revealed that the Congo has deeper storms, a higher reflectivity above the FL in storms (for example, at 7 km), a stronger 85-GHz ice scattering signature, and also more lightning activity, as compared to the Amazon (Boccippio et al. 2000; Petersen and Rutledge 2001; Toracinta et al. 2002). Essentially precipitation systems over the Amazon are more maritime in nature than those over the Congo.

This study describes the vertical structure of precipitation systems in Africa in more detail. The focus is on regional differences in Africa, but a comparison with the Amazon Basin is included, in order to provide a context. Storm systems in the Amazon have been studied in some depth (e.g., Stith et al. 2002; Petersen et al. 2002; Sorooshian et al. 2002), in part thanks to the TRMM Large-Scale Biosphere–Atmosphere (LBA) field campaign in the Amazon. To our knowledge none of the TRMM-based precipitation studies has focused on regional variations in Africa, except two. These two (Adeyewa and Nakamura 2003; Nicholson et al. 2003) compare TRMM-based rainfall estimates to those based on other satellite data and rain gauges. Clearly much research has been conducted into rainfall variability in Africa using other data sources (e.g., Lebel and Amani 1999; Nicholson et al. 2000), but this is beyond the scope of the current study, which focuses on the vertical structure of precipitation systems. That structure has been described for some isolated cases, all large convective systems in West Africa, mainly based on ground-based radar data (e.g., Roux et al. 1984; Chalon et al. 1988; Roux and Sun 1990), but these studies do not represent a climatology of precipitation systems. In short, the typical vertical structure of precipitation systems in various climate regions of Africa remains undocumented. This is the motivation for the present study, which aims to describe the regional, diurnal, and seasonal variations of the vertical structure of precipitation systems in Africa, and to interpret these variations in terms of typical stability and shear profiles. Specifically, *we aim to answer whether the vertical structure of precipitation systems, and its diurnal variation, is different in the distinct climatic zones of Africa, and different from that in the Amazon Basin.*

The broader impact of this study is obvious: the economy of most African countries primarily depends on agriculture, and agriculture in Africa is highly dependent on the performance of precipitation. To better understand rainfall variability, the vertical structure and evolution of precipitation-generating systems needs to be documented, and this information has been unavailable in Africa, in part because of the lack of scanning radar networks. Thus TRMM has come to fill one data void over Africa. This study will also provide a climatological and regional context for the detailed observations of precipitation systems in West Africa, to be collected during the African Monsoon Multidisciplinary Analysis (AMMA, whose field phase is to be conducted in 2006; see online at http://www.joss.ucar.edu/amma).

Following a description of the data sources and analysis method (section 2), the vertical structure of African precipitating systems is presented (section 3). An analysis of the diurnal variation of TRMM PR surface precipitation and storm structure follows in section 4, and the findings of this study are interpreted in the context of regional variations of climatological values of humidity, wind shear, and stability in section 5.

2. Analysis method

a. Data source

The TRMM satellite follows a 35°-inclination non-sun-synchronous low-earth orbit (Kummerow et al.

1998). Its orbit altitude was about 350 km above the earth before August 2001, and 403 km afterwards. Its instruments include a four-frequency microwave radiometer and a 13.8-GHz radar (the PR). The TRMM radar and passive microwave radiometers have been building a superbly calibrated dataset of rainfall rate and vertical structure of precipitating systems over land and ocean since December 1997. The nonsynchronicity with the sun is rather unique compared to other earth observing satellites, and it is important, because over time it enables the deduction of the diurnal variability.

Spaceborne radar observations are superior to ground-based radar data for the description of the storm vertical structure, because of the near-nadir vantage point (Heymsfield et al. 2000; Hirose and Nakamura 2002). They are superior also to a network of ground radars for regional precipitation climatology studies, because there are no range-related problems such as variable resolution, variable minimum echo height, and variable sensitivity, nor are there regional variations in radar calibration (Anagnostou et al. 2001). The drawback of the spaceborne radar observations is the data scarcity: the TRMM PR swath, 220 km wide, visits the same location only once or twice a day (Negri et al. 2002).

The PR's minimum detectable signal is about 17 dBZ (Iguchi et al. 2000). Assuming uniform beam filling, this implies a rain rate of about 0.3 mm h^{-1} (Fisher 2004). The horizontal resolution of the PR is about 4.3 km at nadir, before the orbit boost (5.7 km after the boost). This allows the TRMM PR to observe precipitation systems larger than about 10 km^2 (Wilcox and Ramanathan 2001). Sauvageot et al. (1999) use a ground-based radar to show that less than a quarter of all rain cells in Niger, Africa, have diameters larger than 5 km. If this finding applies generally in Africa, then clearly the storms analyzed in this study are mainly the larger ones: the effects of limited horizontal resolution and low sensitivity combine to exclude isolated, small storm cells from the PR's view (Heymsfield et al. 2000). An attempt has been made to correct for this nonuniform beam-filling effect on PR-based surface rain estimation (Durden et al. 1998), but reflectivity profiles are not "corrected." All this suggests that the present study is biased toward the larger precipitation systems, but then, they carry the bulk of the rain [e.g., Fig. 9.1 in Houze (1993)].

The PR's range resolution is 250 m. Therefore its vertical resolution is 250 m at nadir, decreasing to about 1.6 km (Gaussian weighted) at the outer incidence angle (17°). Because this study focuses on the vertical structure, only the profiles with an incidence angle less than 5° on either side of nadir are included.

The primary dataset for this study is the TRMM-PR 2A25 volumetric radar reflectivity and surface rainfall rate (Kummerow et al. 1998). The 2A25 equivalent reflectivity profiles are corrected for attenuation by heavy rain, mainly using the surface reference technique (Iguchi and Meneghini 1994), and the rain rates are corrected for nonuniform beam filling (Iguchi et al. 2000). The 2A25 surface rain rate is estimated from the near-surface reflectivity, assuming a Z–R relationship specific to the rain type: $Z = 148R^{1.55}$ for convective and $Z = 276R^{1.49}$ for stratiform precipitation. The rain type is defined based on both horizontal and vertical storm structure information, in the 2A23 algorithm. The 2A23 rain type classification itself is not used in this work. This study focuses on the vertical structure of precipitation profiles, irrespective of their classification. Certainly the shape of the reflectivity profiles will reveal stratiform or convective characteristics (Houze 1997; Geerts and Dawei 2004b), but the profiles are not a priori classified.

This study only considers those reflectivity profiles with path-integrated attenuation, that is, with detectable scatterers above the ground. A threshold of 17 dBZ is imposed, even though the 2A25 dataset includes reflectivity values down to 15 dBZ. These are referred to as the precipitation profiles. Most but not all of the precipitation profiles are also surface rain profiles. There is a number "virga" profiles, with echoes stronger than 17 dBZ at some level, but no detectable rain reaching the surface (2A25 surface rain rate equals zero). The fraction of virga profiles is generally less than 20%. The 2A25 reflectivity data are composited as a function of height. This is the height above the standard geoid, which is very close to mean sea level. Especially for the African continent it is important to note that the height shown is not above ground level.

The TRMM 3B42 daily $1° \times 1°$ data are also used in this study to describe the basic seasonal swing of precipitation over Africa. The 3B42 dataset is based on a combination of infrared (IR), passive microwave, and radar data from TRMM and IR data from the geostationary satellites. Finally, for the interpretation of the TRMM data, we use the National Centers for Environmental Prediction (NCEP)– National Center for Atmospheric Research (NCAR) global reanalysis dataset, which is based on upper-air and satellite data (Kalnay et al. 1996). We use monthly mean values of atmospheric variables for the period 1968–96. We obtained these data through the Web site of the U.S. Climate Diagnostics Center (available online at http://www.cdc.noaa.gov).

b. Regional classification

The seasonal march of precipitation in Africa is well established (Fig. 1). Regions between 10° and 25° latitude experience a single wet season peaking shortly after the summer solstice. Precipitation is rare outside of this 3–5-month-long wet season. Regions near the equator tend to have two peaks, at or shortly after the equinoxes, with otherwise little seasonal variation in rainfall.

To make regional comparisons, Africa is categorized into nine broad climatic regions (Table 1). Those re-

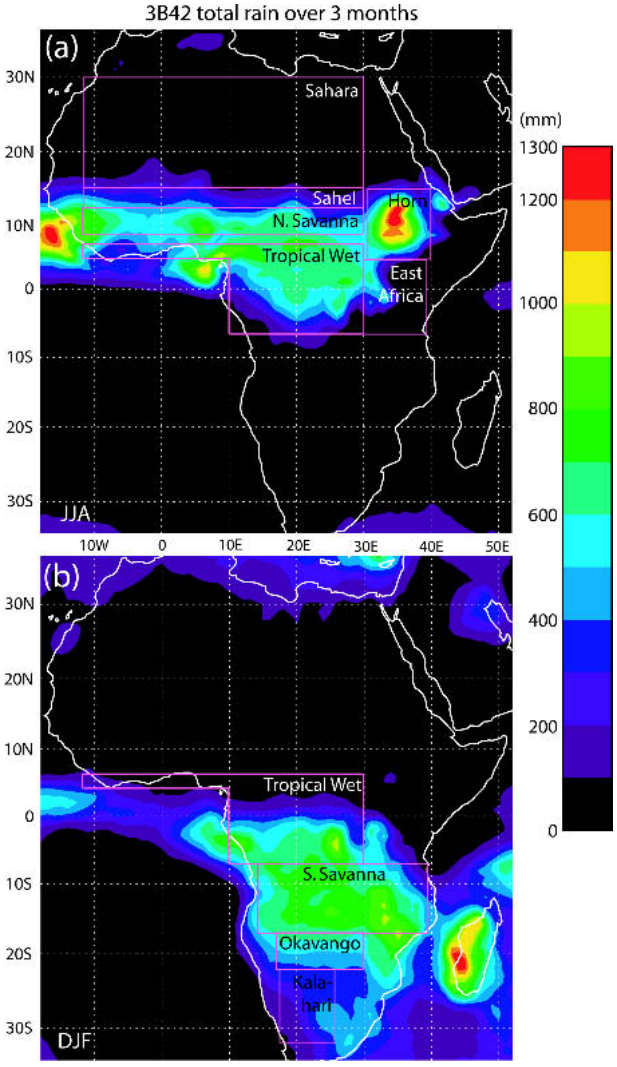

FIG. 1. Mean rainfall over Africa for 1998–2002 based on TRMM 3B42 data. The units are mm in 3 months. Also shown are the geographical regions studied here. (a) JJA and (b) DJF.

ceiving the bulk of the precipitation in the boreal summer are the Sahara (15°–30°N, 11.5°W–30°E), the northern semiarid region (Sahel, 12°–15°N, 11.5°W–30°E), the northern Savanna belt (8°–12°N, 11.5°W–30°E), the Horn of Africa (4°–14.5°N, 31°–40°E), the plateau region of Eastern Africa (6.5°S–4°N, 30°–39°E), and the Tropical Wet region. The latter includes the Congo Basin (6.5°S–6.5°N, 10°–30°E) plus the south coast region of West Africa (4.5°–6.5°N, 11.5°W–10°E); both parts largely have an Am climate in the Köppen classification. At first, the south coast region of West Africa was treated separately from the Congo Basin, but the reflectivity profiles are very similar, so the two regions are combined. In any event, the Tropical Wet region is dominated by the Congo Basin, which occupies 86% of that region. Fifteen months of 2A25 data are used for the six regions shown in Fig. 1a: June, July, and August (JJA) 1998–2002. In some regions the wet season is centered on August rather than July, but the JJA period includes the majority of the precipitation systems in most regions, including the early monsoon convection.

TABLE 1. Summary statistics of the climatic regions in Africa. The Amazon Basin is included for comparison. The number of rain events per unit area is the total over 15 months (3 months in each of 5 yr). The average surface rain rate is conditional (i.e., when it rains at the surface).

	Area (10^6 km^2)	Season	No. of rain profiles per 10^3 km^2	Avg rain rate (mm h^{-1})
Sahara	7.09	JJA	9	4.43
Sahel	1.49	JJA	88	5.06
Savanna North	2.01	JJA	112	4.33
Horn	1.15	JJA	82	4.6
East Africa	1.16	JJA	24	4.59
		MAM	71	4.20
Tropical Wet	3.73	JJA	62	4.45
		DJF	45	5.25
Savanna South	3.16	DJF	113	3.36
Okavango	0.75	DJF	107	3.46
Kalahari	0.93	DJF	73	4.29
Amazon	1.23	JFM	153	2.94

The three remaining regions receive most of their precipitation in the austral summer: the southern Savanna belt (17°–6.5°S, 14°–39°E), the southern semiarid region (Okavango, 22°–17°S, 17°–30°E), and the Kalahari (22°–32°S, 17.5°–26°E). Again fifteen months of 2A25 data are used for these regions: December, January, and February (DJF) 1998–2002 (including December 1997 but excluding December 2002). The Tropical Wet and East Africa have year-round precipitation somewhere within their respective regions, and neither the JJA nor the DJF periods capture the wettest periods. For the Tropical Wet region, we include both JJA and DJF periods. For East Africa we include both the JJA period, which is relatively dry except in the northwestern part (Fig. 1a), as well as the MAM (March–April–May) period, because it is the wettest 3-month period for the entire region. The winter-wet season in the Mediterranean climates of northern Africa and the southwestern corner of Africa is ignored in this study, because the precipitation systems are extratropical. Finally, we included the central Amazon Basin well inland from the coast (1°–11°S, 65°–55°W), because the Amazon is relatively well-studied (see section 1), thus its PR data provide a context for the African data. The wettest period in the central Amazon is the JFM period.

This regional classification is mainly based on the distinct rainfall climatology of each region (Fig. 1). It is rather standard (e.g., Leroux 2001) and similar to that by Adeyewa and Nakamura (2003). The latter study ignores the Horn, East Africa, and the Kalahari. The regional boundaries are a simplification of the regionalization by Nicholson and colleagues (e.g., Nicholson

et al. 2000). Clearly the regions defined in this study do not have the same incidence of precipitation systems (Table 1): the Sahara for instance encounters some 12 times fewer rain events per unit area than does the northern Savanna. Yet when it rains, the average surface rain rate is about the same in these two regions, and indeed in all regions in Africa.

c. Analysis of diurnal variability

Determining the diurnal variability of precipitation matters, not only because it places fixed-time rainfall estimates from other polar-orbiting satellites, on a sun-synchronous orbit, in a diurnal context (Bell and Reid 1993), but also because it helps to understand the dynamics of precipitating systems in response to diurnally varying surface energy fluxes and lower-tropospheric wind profiles (e.g., Dai et al. 1999). The diurnal variability of precipitation is not captured well by operational numerical weather prediction models (e.g., Davis et al. 2003) or general circulation models (e.g., Lin et al. 2000), in part because convection is parameterized. The diurnal variation of precipitation, as observed by satellite or rain gauges, has received much attention [see Dai (2001) for a review], but the focus here is on the diurnal variation of vertical storm structure.

To study the diurnal variation, reflectivity profiles and surface rain rates are binned at a 3-h temporal resolution. The TRMM orbit is such that the chances of an overpass are about equal for each 3-h bin, over the course of a month or longer. Comparison with a dense network of rain gauge data in Oklahoma has shown that the TRMM PR captures the diurnal variation of the surface rain well (Fisher 2004; B. Fisher 2004, personal communication). A 3-h bin size is rather course, but it allows maximization of the sample size. A temporal resolution of 1 h, even using three years of PR data, is inadequate to describe the local (single pixel) diurnal cycle of precipitation due to spatially inconsistent sampling (Negri et al. 2002). Spatial averaging over rather large regions of course allows a finer time resolution. Considering the large size of the climatic regions selected for this study (Table 1) and the 5-yr data period, temporal sampling was done every 3 h, which is a trade-off between statistical significance and the ability to capture the true diurnal variability. The number of samples (TRMM PR profiles with path-integrated attenuation) per 3-h time bin averages 18 10^3 (this can be inferred from columns 2 and 4 in Table 1) and ranges between 1339 (East Africa, 0600–0900 LT[1] and 55 038 (Savanna South, 1500–1800 LT). Thus the sample size appears sufficient to study diurnal variability.

3. Regional variability of the vertical structure of precipitation systems in Africa

a. Composite vertical structure

The probability density function of radar reflectivity as a function of height is shown in Fig. 2 for regions with mainly JJA rainfall and in Fig. 3 for regions with rain mainly in DJF. Shown in these frequency-by-altitude diagrams (FADs) is the probability $N(Z, h)$ for a given reflectivity Z (in dBZ units) at a certain height h, normalized such that the sum of all frequencies plotted equals 100—that is, $\Sigma_Z\Sigma_h N(Z, h) = 100$. The FADs include all attenuated profiles. The FADs are truncated on the left due to the PR's limited sensitivity, so the entire reflectivity distribution, as shown for instance in Geerts and Dawei (2004b), is not known. The FADs are further partitioned between light surface rain (<8 mm h^{-1}) and heavy surface rain (>8 mm h^{-1}).

A first observation is that *the regional differences in the vertical structure of precipitation systems in Africa are relatively small*. Precipitation systems appear generally deep; relatively large or numerous hydrometeors are found high above the FL. In most regions echoes between 17 and 25 dBZ are more common at 6 km, above the FL, than at 3 km. Even light surface rainfall events (less than 8 mm h^{-1}) are generally associated with deep precipitation columns. In some regions, especially the Sahara (Fig. 2, upper-left graph), a surface rain rate less than 8 mm h^{-1} often seems to be associated with low-level evaporation. In general low-level evaporation is suggested by the more frequent occurrence of higher reflectivities near 4 km, as compared to levels closer to the ground. As a result, frequency isolines just below the FL tilt to the left toward the ground in several regions. More steeply tilting isolines are present in the FADs for systems with a surface rain rate less than 4 mm h^{-1} and less than 2 mm h^{-1} in the Sahel and Sahara (not shown). Such tilt is absent in more humid regions, such as in the Savanna South (Fig. 3) and in the south coast region of West Africa, part of the Tropical Wet region in JJA. On the other hand, some frequency isolines below the FL slightly tilt to the right in the Amazon region, indicating low-level rain drop growth by collision–coalescence, and a low cloud base (Fig. 3).[2]

A shift to the right (higher reflectivities) can be seen in a thin layer at a height of about 4.5 km (that is, near the FL) in most FADs. This is associated with the occurrence of a bright band, a signature of stratiform precipitation. The brightband spike is better defined for the light rain cases, suggesting that the light rain group

[1] For each reflectivity profile, the local solar time (LT) is used instead of universal time (UTC) because it is the relevant time in the description of the diurnal variation. The local solar time is such that the sun is highest in the sky at local solar noon.

[2] Some caution is warranted in the interpretation of the FAD at low levels. In regions with much elevated terrain—such as East Africa, the Horn, the southern Savanna, the Okavango, and the Kalahari—the rapid decay of frequencies between 1- and 2-km height obviously is related to the terrain.

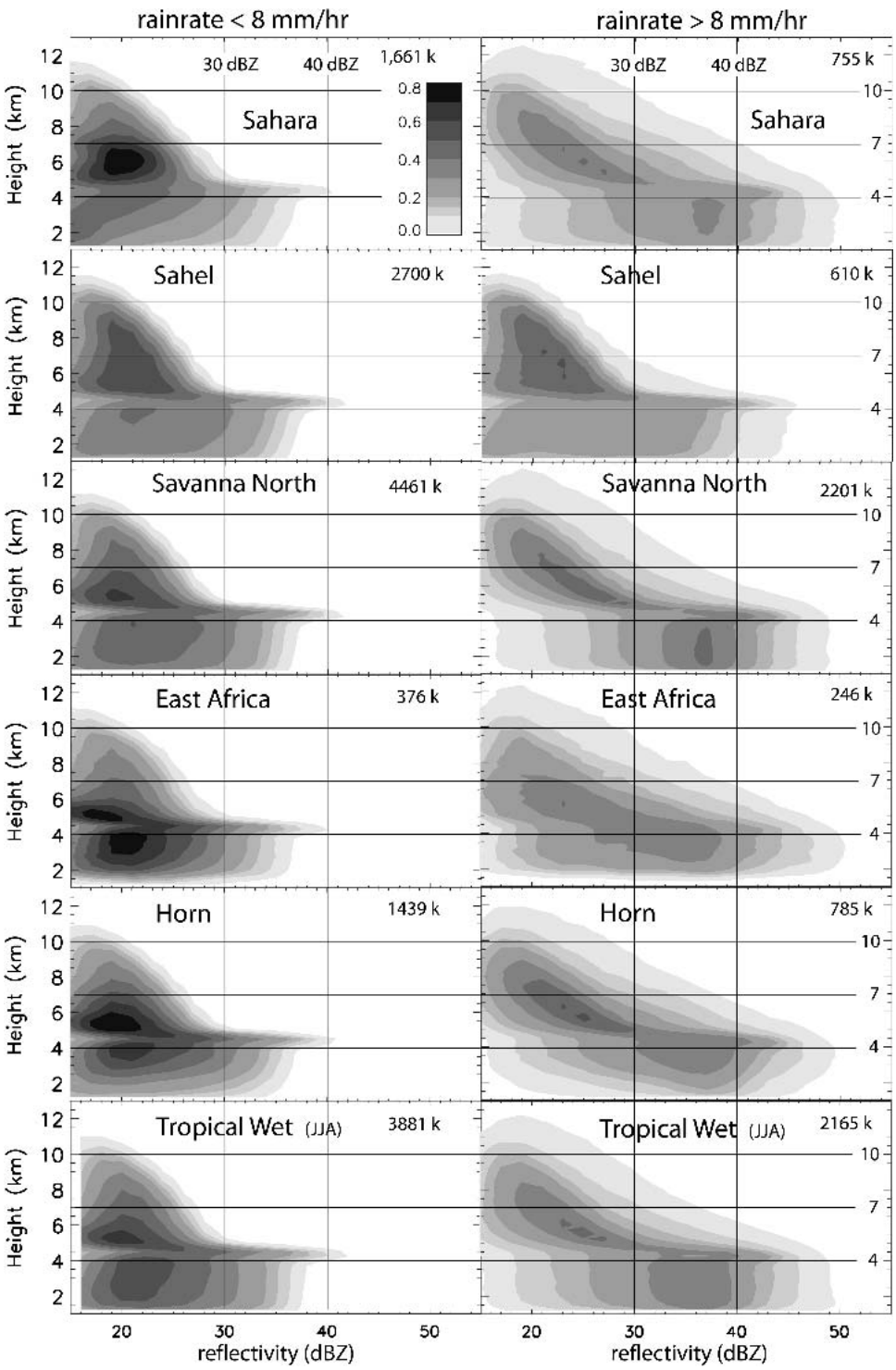

FIG. 2. Probability density functions of reflectivity-by-altitude for all cases with PR-detected surface rain rate (R) (left) $0 < R \leq 8$ mm h^{-1} and (right) $R > 8$ mm h^{-1} for all regions with a JJA wet season, based on JJA 1998–2002 2A25 data. The probability is normalized, i.e., it is the number of occurrences per 2 dBZ per 250 m, divided by all occurrences in all reflectivity and height bins, and expressed as a percentage. The total number of occurrences is shown in the upper-right corner of each plot, in thousands. Vertical lines are drawn at 30 and 40 dBZ, and horizontal lines at 4-, 7-, and 10-km height.

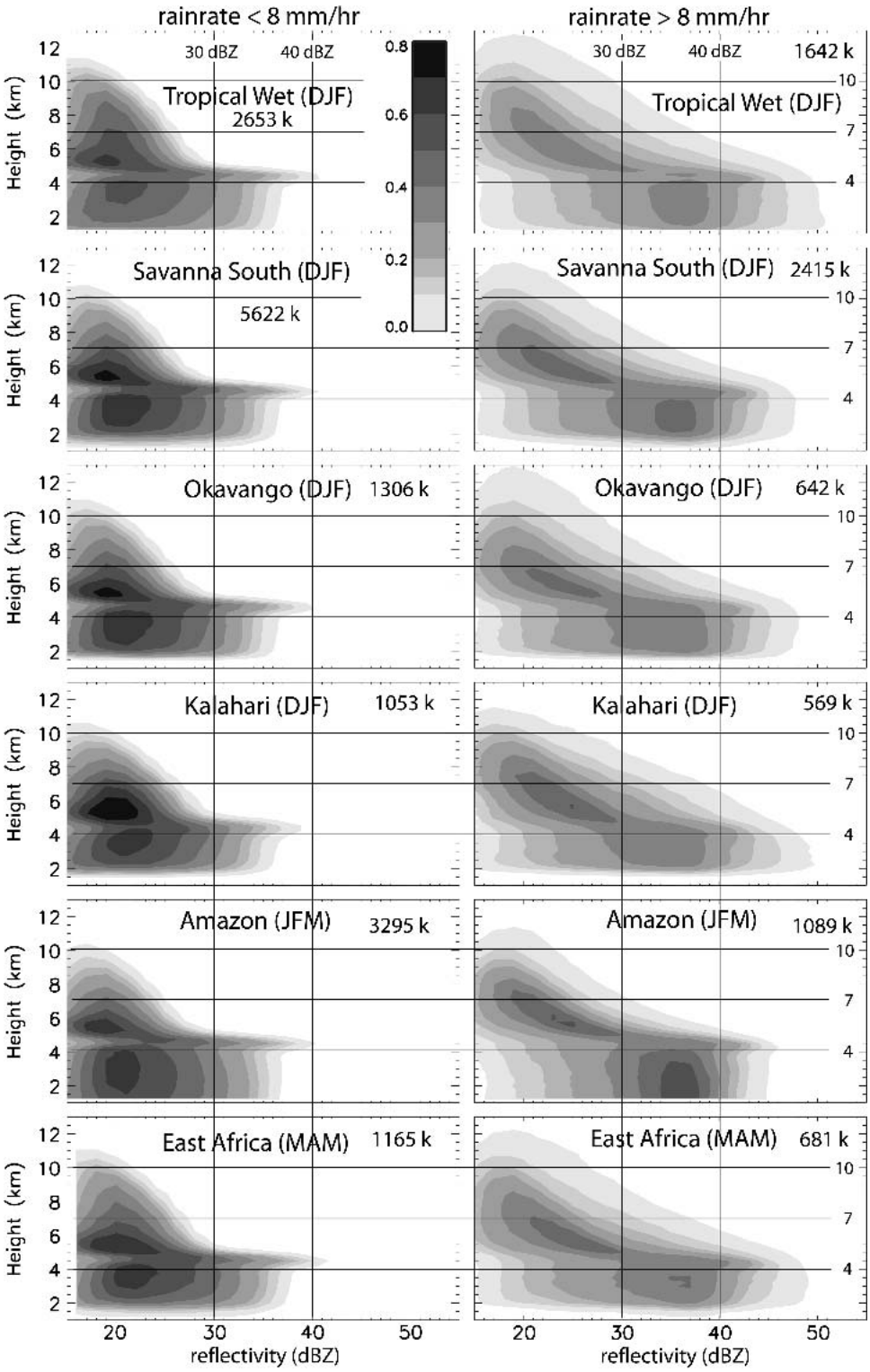

FIG. 3. As in Fig. 2, but for the regions with a DJF wet season. Also included here are East Africa (MAM) and the Amazon Basin (JFM).

TABLE 2. Frequency of virga and of warm rain, expressed as a percentage of all precipitation profiles.

Region—season	Virga	Warm rain
Sahara—JJA	28	2.9
Sahel—JJA	16	3.1
Savanna North—JJA	15	5.7
Tropical Wet—JJA	12	9.7
East Africa—JJA	12	9.0
Horn Africa—JJA	13	3.1
Kalahari—DJF	15	6.4
Okavango—DJF	13	6.7
Savanna South—DJF	12	7.2
Tropical Wet—DJF	15	7.4
East Africa—MAM	10	8.0
Amazon—JFM	10	16.7

has a larger fraction of stratiform precipitation. It is well-defined in the Amazon, although not better than in some African regions, such as the Tropical Wet in JJA. It is absent in case of heavy rain in many regions (e.g., the Horn and East Africa in JJA, or the Tropical Wet in DJF), suggesting that the heavy rain there is largely convective. In the Horn and East Africa these may be mostly orographically controlled precipitation systems that do not develop much mesoscale organization. The brightband spike is least defined in the desert regions (Kalahari and Sahara) and best defined in the Sahel and northern Savanna regions, where it can be seen even in the heavy rain cases. This may be due to the occurrence of large mesoscale convective systems and associated stratiform regions there (e.g., Roux et al. 1984; Chalon et al. 1988). Storms producing heavy rain differ little regionally in terms of vertical structure. Over the northern arid and semiarid regions they tend to be a little deeper, and have higher reflectivities aloft, than in the Tropical Wet region, but the FADs are quite similar.

The FADs discussed above includes profiles in which rain does not reach the ground. The fraction of virga profiles varies from 10% in the Amazon, 10%–16% in all regions of Africa (except the Sahara), to 28% in the Sahara (Table 2). Virga-producing storms are often quite deep, but their peak reflectivity is generally below 30 dBZ (Fig. 4). In arid regions such as the Sahara, the virga profiles tend to be more top-heavy than in the Tropical Wet, in terms of the vertical distribution of reflectivity, and thus they may have a larger ice hydrometeor concentration and a stronger 85-GHz ice scattering signature than in the Tropical Wet. This, plus the higher virga fraction in the Sahara implies that passive-microwave–based surface rain-rate estimations may be too high in the Sahara.

In all regions the virga FADs show a spike at the FL, more so in the Tropical Wet than the Sahara. This spike is more clearly defined than in the corresponding FADs for light rain events (<8 mm h^{-1}; Fig. 2), suggesting that virga profiles are often stratiform. Many of the virga profiles may be associated with mesoscale convective systems in their mature to dissipating stages (Smull and Houze 1987; Houze 1997). Mesoscale convective complexes are more common in the Sahara, Sahel, and northern Savanna than in other regions (Laing and Fritsch 1993). This may contribute to the relative prevalence of virga profiles in these regions (Table 2).

b. Storm intensity

To further compare and contrast the typical vertical storm structure in various regions in Africa, we examine the frequency distribution of reflectivities as a func-

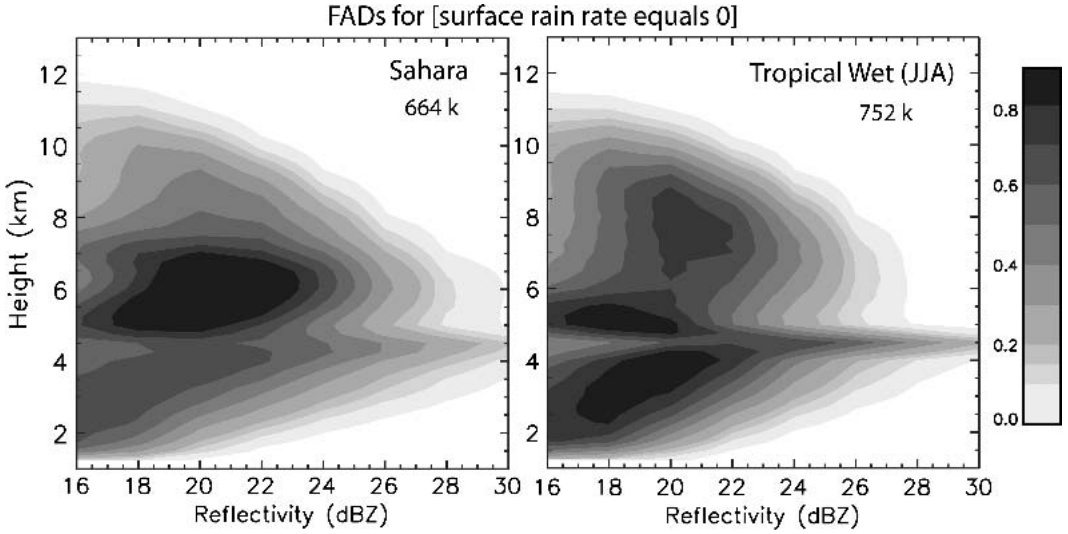

FIG. 4. As in Fig. 2, but for virga profiles only, in the Sahara and the Tropical Wet (JJA) region. Note that the maximum reflectivity plotted is only 30 dBZ. The last contour peaks at 32 dBZ in the Sahara and 33 dBZ in the Tropical Wet region.

tion of height, for various exceedance levels (Fig. 5). The frequencies are divided by the total number of precipitation profiles in each region, so Fig. 5 shows the probability of a reflectivity of at least the threshold value (17, 27, or 37 dBZ) as a function of height. Such PDFs are preferred over mean reflectivity profiles, because the calculated mean reflectivity will be above the true mean if only the measured population (>17 dBZ) is included in the average, and below the true mean if all profiles are included and the unsampled population (<17 dBZ) is given an arbitrary value, for example, $Z = 0$ mm^6 m^{-3}. Also, even if the PR were able to measure the full reflectivity spectrum, the mean reflectivity at any level is based a decreasing sample size in the upper troposphere, thus its profile does not represent the same population at all levels, and at its highest level it only represents the deepest storm. In short, mean reflectivity profiles are not very meaningful. To assess sensitivity to the normalization method, the frequencies shown in Fig. 5 were normalized also by the total number of reflectivity occurrences at all levels (listed in Figs. 2 and 3), and the results are essentially the same. The maxima remain <100% in the left panels of Fig. 5, because there may be precipitation profiles (possibly virga) that do not have a detectable echo at the level of these maxima.

We also examine the mixing ratio q_h of hydrometeors (Fig. 6). Hydrometeors are defined here as rain or snow large and widespread enough within the PR footprint to produce an echo of at least 17 dBZ. This mixing

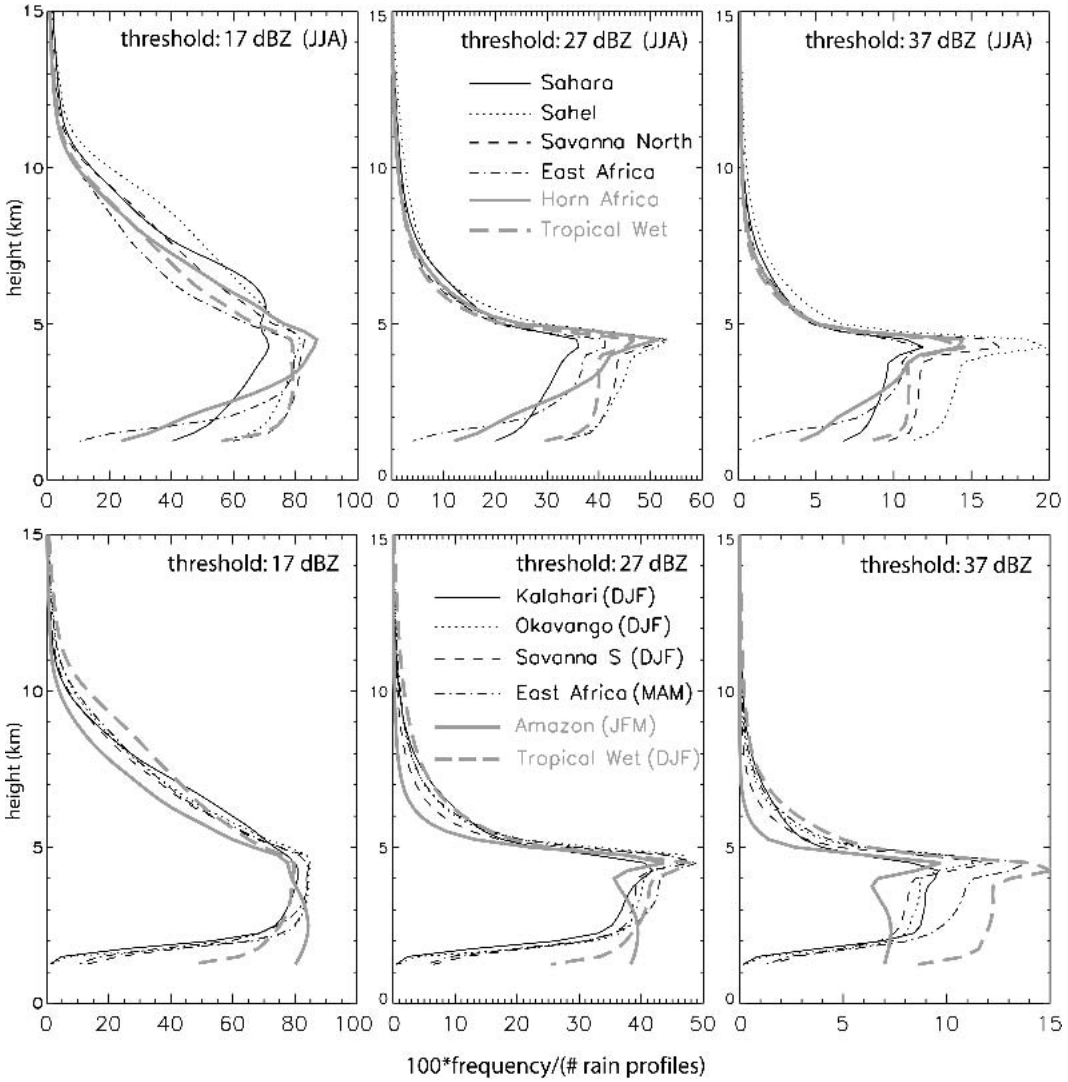

FIG. 5. Frequency distribution of reflectivity values with height. Three thresholds are used: (left) 17, (middle) 27, and (right) 37 dBZ. (top) JJA regions and (bottom) DJF regions. Note that the range displayed along the x axis varies.

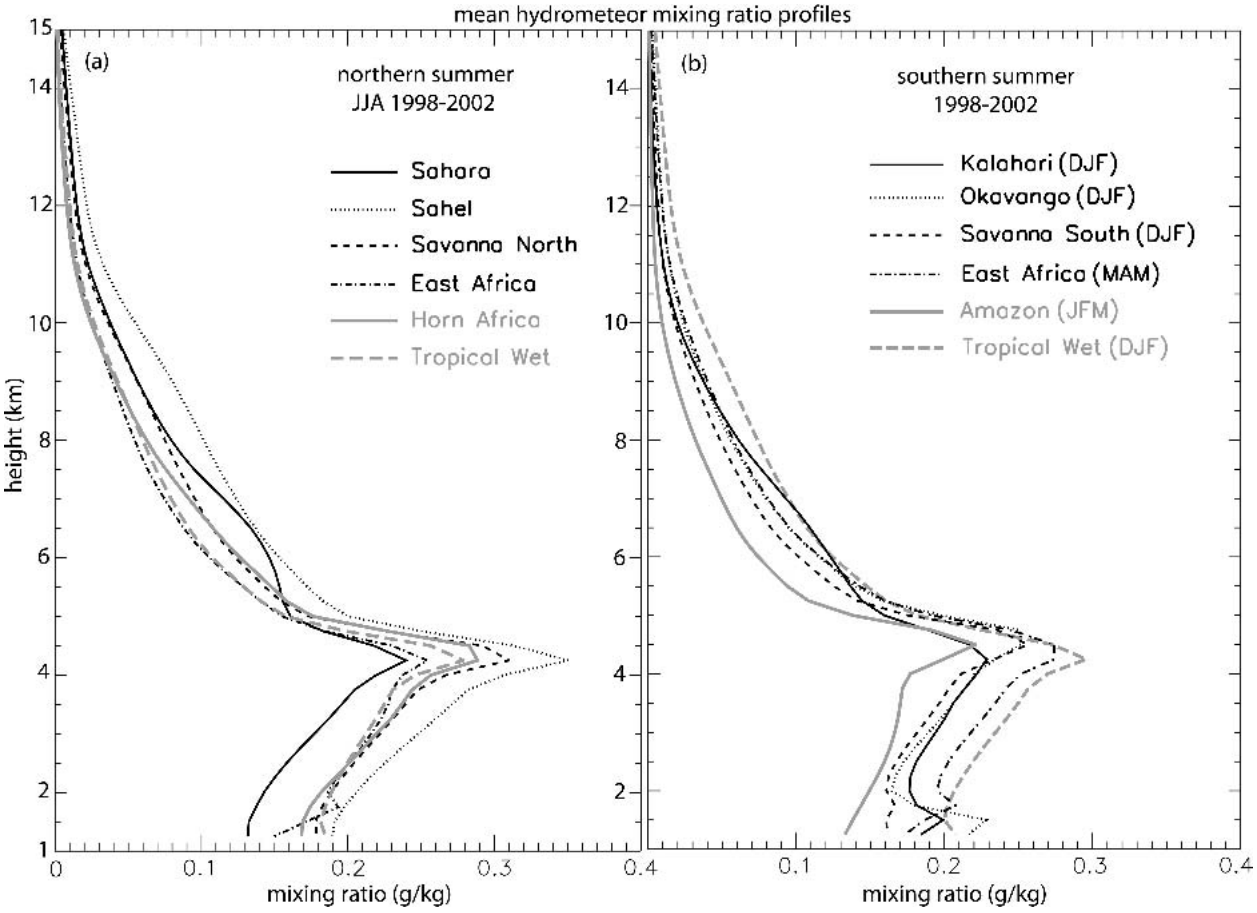

FIG. 6. Profiles of hydrometeor water content for all regions. See text for details. (a) JJA regions and (b) DJF regions.

ratio q_h (g kg^{-1}) is derived from an empirical Z–q_h relationship,

$$q_h = 3.2 * 10^{-3} Z^{0.55} e^{h/8} \quad \text{(rain: for } h < 4.5 \text{ km)}, \qquad (1a)$$

$$q_h = 6.8 * 10^{-3} Z^{0.45} e^{h/8} \quad \text{(snow: for } h \geq 4.5 \text{ km)}, \qquad (1b)$$

where h is the height in km, Z the equivalent reflectivity in mm^6 m^{-3}, and e the exponent. The constants are based on Eqs. (7.13c) and (7.13d) in Battan (1973) for liquid and frozen hydrometeors in an array of summertime precipitation systems in North America. These relationships are experimental, and no effort was made to validate them. We are merely interested in the regional variation of the profile and the vertically integrated amount, as a proxy for the true hydrometeor water contents in storms in Africa.

Some interesting regional differences appear in the vertical storm structure in Africa. The Sahel region experiences the most intense storms, in terms of the frequency of echo strength above 7 km, the occurrence of strong echoes at low levels (Fig. 5), and the hydrometeor content (Fig. 6). The Sahara storms tend to be nearly as intense aloft (especially near 6 km), but the low-level reflectivity is lower, and the kink at the FL is less defined, as compared to the Sahel. The Tropical Wet region tends to have deeper, more intense storms in the southern summer than the northern summer; in fact, the deepest, most intense storms in the southern summer tend to be found in the Tropical Wet region, mostly in the southern Congo Basin. The average conditional rain rate at the ground in DJF in the Tropical Wet region is higher than elsewhere, even the Sahel (Table 1).

In general the northern zenithal rain regions (Sahara, Sahel, and Savanna) tend to have deeper storms than their southern counterparts (Kalahari, Okavango, and southern Savanna, respectively) (Figs. 2, 3, 5). Echo frequency generally decreases for all thresholds in Fig. 5 from below the FL to a level still above the terrain in all regions of Africa (say 2 km). This suggests evaporation (or breakup) of raindrops.

A clear difference does exist between storms in any African region and those over the Amazon: Amazon storms tend to be more shallow and their mean profile has a more stratiform appearance than in Africa, with a clear brightband maximum in the 27- and 37-dBZ thresholds (Fig. 5) and a remarkably rapid decay of

reflectivity counts with height above the bright band. Rain events are quite frequent in the Amazon (Table 1), but the average conditional rain rate at the ground, as derived by the PR, is lower than in any African region (Table 1), which is consistent with the low hydrometeor mixing ratio in the Amazon near the ground (Fig. 6b). Also, the reflectivity counts in the Amazon tend to increase from 4 km down to 2 km for all thresholds (Fig. 5). This unusual property suggests that rain drops grow toward the ground, which may imply a low average cloud base in the Amazon region.

c. *Echo tops*

The regional variation of echo tops is shown in Fig. 7. The echo top is defined for each profile as the highest occurrence of the 20-dBZ contour. The value of 20 dBZ is close to the minimum detectable signal and it has been used elsewhere (e.g., Toracinta et al. 2002). In addition to the echo top distributions for the various regions, Fig. 7 also shows the distribution inferred from Short and Nakamura (2000, their Fig. 2). That study uses the TRMM 3A25 (monthly mean) parameter "storm height, " which is the highest measurable echo at the PR sensitivity, for all storms over land between 30°N and 30°S for JJA and DJF 1998. The Short and Nakamura (2000) curves correspond with the echo top PDFs in Africa (Fig. 7).

The 20-dBZ echo top is clearly most likely to occur near the FL in most regions in Africa. Short and Nakamura (2000) confirm the existence of this maximum over all tropical land regions; however, their maximum is less spiked, because their vertical resolution is worse (500 m). The peak near the FL may represent a population of warm cumulus congesti, which have been shown to be important over tropical oceans (Johnson et al. 1999). Or they may be rather weak stratiform precipitation regions with snow aloft, but too weak to be detected above the bright band. The PR horizontal resolution may also contribute: even intense storms,

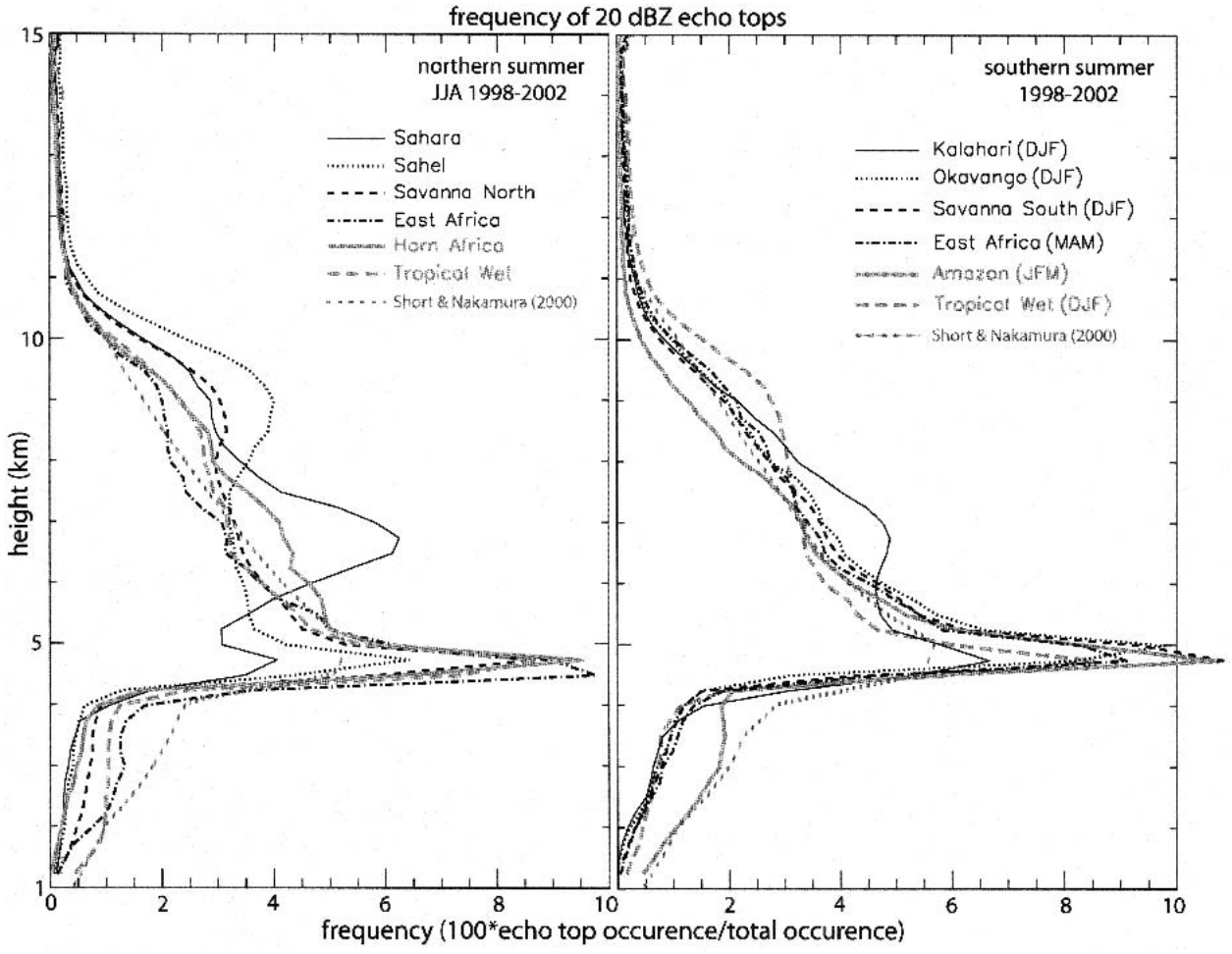

FIG. 7. Probability density functions of 20-dBZ echo tops for all surface rain profiles. The probability is normalized, i.e., it is the number of occurrences per 250 m, divided by all occurrences in all height bins, and expressed as a percentage. PDFs inferred from Short and Nakamura (2000) are shown as well, for both seasons.

smaller than the PR footprint, may only become detectable near the FL (Heymsfield et al. 2000). This clustering of 20-dBZ echo tops near the FL is most pronounced in the Amazon (Fig. 7), where high reflectivity values above the FL are rare, even in heavy rain events (>8 mm h^{-1}; Fig. 3).

Within Africa, a remarkable difference exists between storm depths in the arid regions and those elsewhere (Fig. 7). The Tropical Wet, Savanna, East Africa, Horn, and Okavango regions all have a single maximum echo top at the FL. The Sahara and Kalahari regions have a peak just below 7 km. The secondary echo top maximum at 9 km in the Sahel is another confirmation that storms there are most intense (Figs. 5, 6). Deep, vigorous storms are also common in the Tropical Wet region in the southern summer (Figs. 5, 7). These observations will be interpreted in terms of climatological thermodynamic profiles in section 5.

Shallow, warm-rain events are relatively rare in Africa. Warm-rain events are defined as those PR profiles with rain at the surface *and* a 17-dBZ echo top below 4.25 km, the lowest level that may be affected by the brightband maximum (Fig. 7). Warm rain is 2.5 times more likely in the Amazon than in the African regions, on average (Table 2). In fact, the Amazon echo top distribution has a secondary maximum below the FL (Fig. 7), something that is more clearly established over the tropical oceans (Short and Nakamura 2000). This confirms that Amazon precipitation profiles are more maritime in character than those in Africa.

Warm rain is less common in the arid, semiarid, and savanna regions of the north than in the corresponding climatic regions in the south (Table 2). This is especially remarkable since the southern part of the continent is about 1.5-km high, thus warm-rain processes are confined to a more shallow depth. In Africa warm rain is most common in the Tropical Wet region, especially in JJA. An FAD of the warm-rain profiles in this region (Fig. 8) shows that reflectivity increases from the echo tops toward the lowest levels. This reflectivity profile is consistent with a low cloud base and growth by collision/coalescence. A similar composite reflectivity profile has been documented for warm-rain events in the Amazon (Geerts and Dawei 2004b).

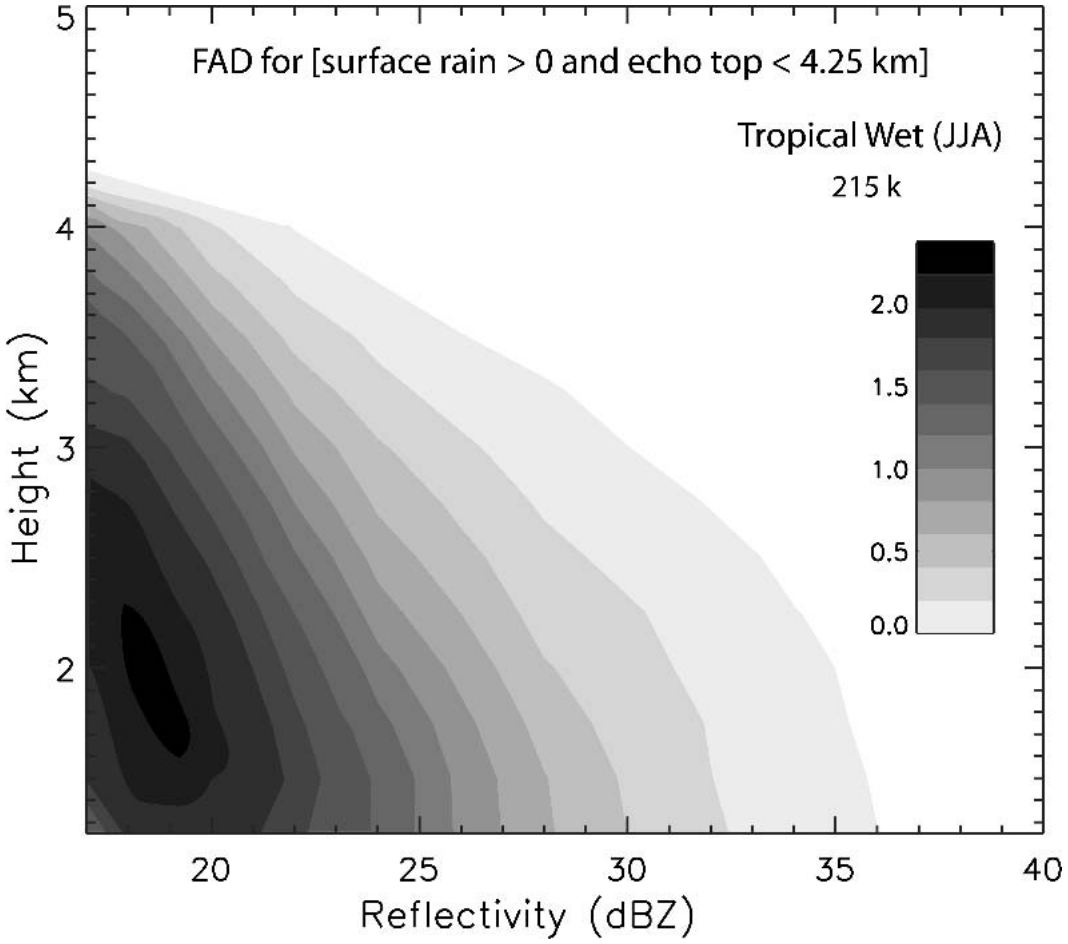

FIG. 8. As in Fig. 2, but for warm-rain profiles only, in the Tropical Wet (JJA) region.

d. Indices of vertical storm structure

Some indices are derived to facilitate a comparison of the characteristic vertical storm structure between regions (Table 3). The *evaporative index* (EI) is defined as the reflectivity at 4.0 km minus that at 2.0-km height. The 4.0-km level is the highest one not contaminated by a bright band, and the 2.0 km is the lowest one above the Earth surface in most places of Africa. A rapid decrease in reflectivity from 4 km down to 2 km, at a scale resolved by the PR, is likely to indicate evaporation of raindrops. The EI is computed for each individual profile in dBZ units, and profiles with reflectivity values below the PR's threshold sensitivity at either level are ignored.

The *stratiform index* (SI) is defined as the reflectivity at 7.0 km minus that at 4.5-km height. The average FL during the wet season in tropical Africa is 4.5–4.6 km; therefore, the 4.5-km level is the most likely location of a bright band, as is evident in Fig. 2. This index is called the stratiform index, because it combines two characteristics of stratiform precipitation: the presence of a bright band, and the rapid decay of reflectivity above the bright band (Geerts and Dawei 2004a). Just as the EI, the SI is computed for each profile as a difference in dBZ units. Again profiles with reflectivities below the PR's threshold sensitivity at 7 km or at 4.5 km are ignored.

The *hydrometeor precipitable water* (HPW) is defined as the vertically integrated liquid or frozen hydrometeor content, and is expressed as a depth of water (mm):

$$\mathrm{HPW} = \frac{1}{\rho_l}\int_0^{\mathrm{top}} \rho q_h \, dz, \tag{2}$$

where ρ_l is the density of water ($\rho_l = 10^3$ kg m^{-3}) and ρ is the density of air (kg m^{-3}). The mixing ratio q_h (g kg^{-1}) of rain and snow is estimated from reflectivity using Eq. (1). Finally, the *storm productivity index* (SPI) is defined as the ratio of the surface rain rate R (mm h^{-1}) over the vertically integrated hydrometeor content HPW:

$$\mathrm{SPI} = \frac{\rho_l R}{\displaystyle\int_0^{\mathrm{top}} \rho q_h \, dz}. \tag{3}$$

The SPI has units of h^{-1} The rain rate R is a PR-based variable in the 2A25 files. While the HPW is affected by the drop-size distribution (rain type), the SPI is rather insensitive to uncertainties in mean drop size, because it is a ratio [see section 2a and Eq. (1)]. The larger the SPI, the more rain is generated by a storm with a given reflectivity profile. Shallow storms have a higher SPI than deep ones. The SPI of storms over high terrain also tends to be higher because of the reduced depth of the reflectivity profile. In both cases the cloud base tends to be closer to the ground, thus less low-level evaporation occurs. Therefore the SPI is somewhat related to the precipitation efficiency of a storm, which is the ratio of the amount of precipitation at the surface to the amount of liquid or frozen cloud water generated by the storm (Hobbs et al. 1980).

The exact values for both the HPW and the SPI are of little meaning, given the uncertainty of the q_h–Z relationships [Eq. (1)]. The indices are used merely to highlight regional differences. All indices listed above, including the EI, are based on profiles with surface rain.

The regional variation of these indices is summarized in Table 3. Storms in the Sahara carry much water above the FL, producing a low SI, yet much water evaporates before reaching the ground, yielding the highest EI (Table 3) and virga fraction (Table 2) of all regions, yet the lowest SPI. The Sahel has a low SPI as well, but that is due more to the great depth of the storms (Fig. 5; i.e., the high HPW, than to low-level evaporation; Table 3). From the arid regions in both hemispheres toward the Tropical Wet, the EI and the virga fraction steadily decrease and the SI generally increases. On exception is that the SI is slightly higher in the Savanna regions (north and south) than in the Tropical Wet. This is consistent with the fact that during the respective wet seasons, the savanna regions are wetter than the Tropical Wet (Table 1). The EI and virga fraction are higher in the northern regions (JJA) than in the corresponding regions south of the equator (DJF), which is consistent with differences in warm-rain fraction (Table 2). The SI is roughly the same in corresponding regions across the equator. The SPI tends to be higher in the equatorial regions, especially in the Horn and East Africa, where the terrain is higher. The higher terrain is also consistent with the higher SPI in the southern regions than the corresponding northern regions.

The fractions in Table 2 and indices in Table 3 highlight how distinct the Amazon is compared to any region in Africa: the EI is negative (low-level rain

TABLE 3. Mean values of the EI (between 4 and 2 km), the SI (between 4.5 and 7 km), the HPW, and the SPI for the various regions and seasons. See text for the definition of these indices.

Region—season	EI dBZ	SI dBZ	HPW mm	SPI h^{-1}
Sahara—JJA	1.99	6.8	0.82	3.11
Sahel—JJA	1.52	9.7	1.11	3.12
Savanna North—JJA	0.99	10.4	0.96	3.39
Tropical Wet—JJA	0.76	9.8	0.74	4.12
East Africa—JJA	0.68	8.8	0.71	4.71
Horn Africa—JJA	1.17	10.0	0.79	4.25
Kalahari—DJF	1.2	7.3	0.72	3.89
Okavango—DJF	0.74	9.7	0.74	3.58
Savanna South—DJF	0.64	10.6	0.71	3.64
Tropical Wet—DJF	0.57	10.1	0.87	3.8
East Africa—MAM	0.68	10.5	0.80	4.09
Amazon—JFM	−0.35	11.6	0.65	3.98

growth) and the virga fraction is low. Storms tend to be relatively shallow and weak, with a high warm-rain fraction and a strong stratiform signature, implying a high SI and a low HPW. Only the SPI is similar to that in Africa, because the impacts of the typically low rain rates (Table 1) and the low HPW cancel each other.

4. Diurnal variability

a. 2A25 surface rain rate

The diurnal cycle of the average 2A25 surface rain rate (R) during rain events is shown in Fig. 9. Heavy rainfall is most likely in the afternoon and evening over most regions in Africa. In most regions the peak rainfall occurs during the 1500–1800 LT period. It is possible that the diurnal variation of the TRMM PR surface rain is partly due to the variation in mean drop diameter (D), since the reflectivity factor $Z \sim D^6$: afternoon convective rain may have a larger mean drop size than late-night precipitation (A. Tokay 2004, personal communication). The change in mean drop size is accounted for, somewhat, by applying a different Z–R (rain rate) relationship for different rain types, convective or stratiform (section 2a). Nevertheless, the possibility remains, and the diurnal variation in rain amount (Fig. 10) may be due more to a variation in rainfall frequency than one in rain rate (Dai 2001). No attempt is made to compare PR-based surface rain data to passive microwave rainfall over Africa.

The sunrise-to-noon quartile is the most suppressed in terms of both rain rate and rain amount in all regions. The diurnal modulation of rain rate and rainfall amount is strongest in East Africa (JJA) and the desert regions (Kalahari, Sahara). Within Africa, it is weakest in the Tropical Wet region. It is even weaker in the Amazon, at least in terms of rain rate. The radar-based study of Rickenbach (2004) describes a similar, slightly higher diurnal rain-rate variation, although the region, Rondonia, is only partially within the Amazon box as defined in this study.

A single 1500–1800 LT peak dominates in the mountainous region of East Africa (JJA), again both in terms of rain rate and rain amount. The semiarid regions in the north (Sahel and northern Savanna) peak later (1800–2100 LT); those in the south (Okavango and southern Savanna) peak earlier (1200–1500 LT). A secondary nocturnal peak in rain rate (Fig. 9) and rain amount (Fig. 10) is observed in the Tropical Wet region, both in the Congo Basin and in the south coast region of West Africa (Fig. 1), in both seasons (DJF and JJA). These secondary peaks occur between midnight and sunrise. It is not clear what causes this secondary maximum in the Congo Basin, but in the West African coastal strip that secondary maximum is due mostly to convection offshore, such as over the Bay of Benin, which is included in the coastal strip. The primary maximum there corresponds with onshore convection, possibly triggered by a sea-breeze circulation (Fig. 11). This see-saw in coastal convective precipitation has been described by means of radar or passive microwave data in this region (Negri et al. 1994) and elsewhere in the Tropics (Houze et al. 1981; Dai 2001; Mapes et al. 2003). The diurnal see-saw in the coastal strip is slightly offset compared to the diurnal peaks in the Tropical Wet region (Fig. 10): the offshore peak is delayed until 0600–0900 LT, that is, after sunrise, and

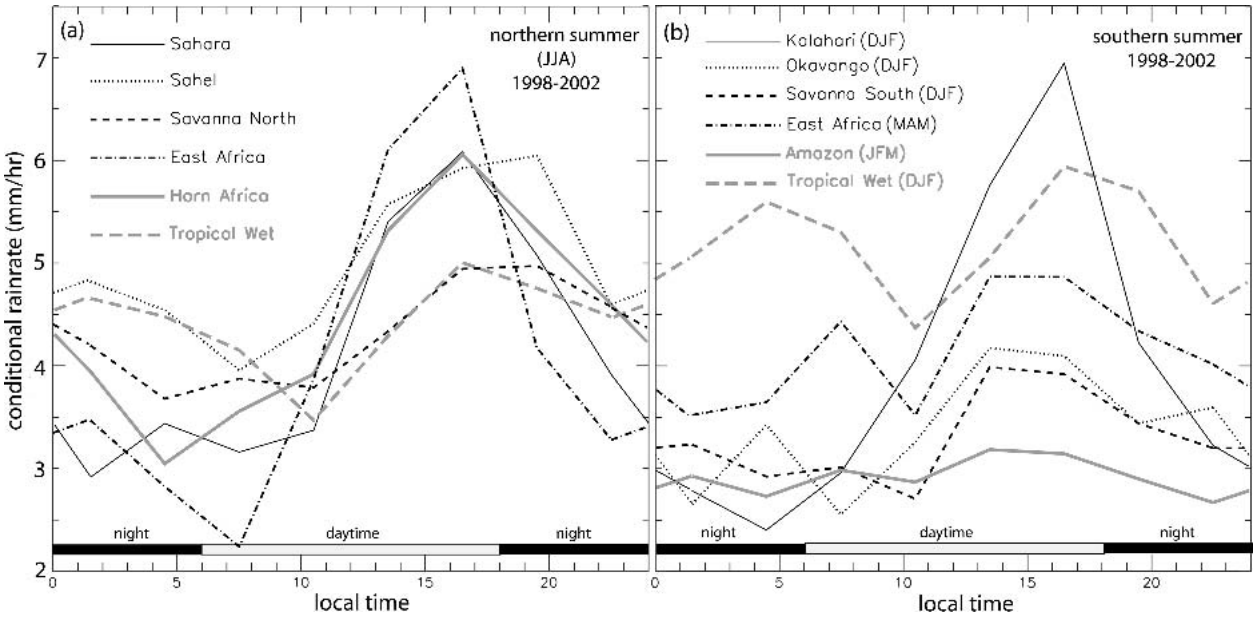

FIG. 9. Diurnal variation of the average surface rain rate, when rainfall is detected, for (a) JJA regions and (b) mostly DJF regions.

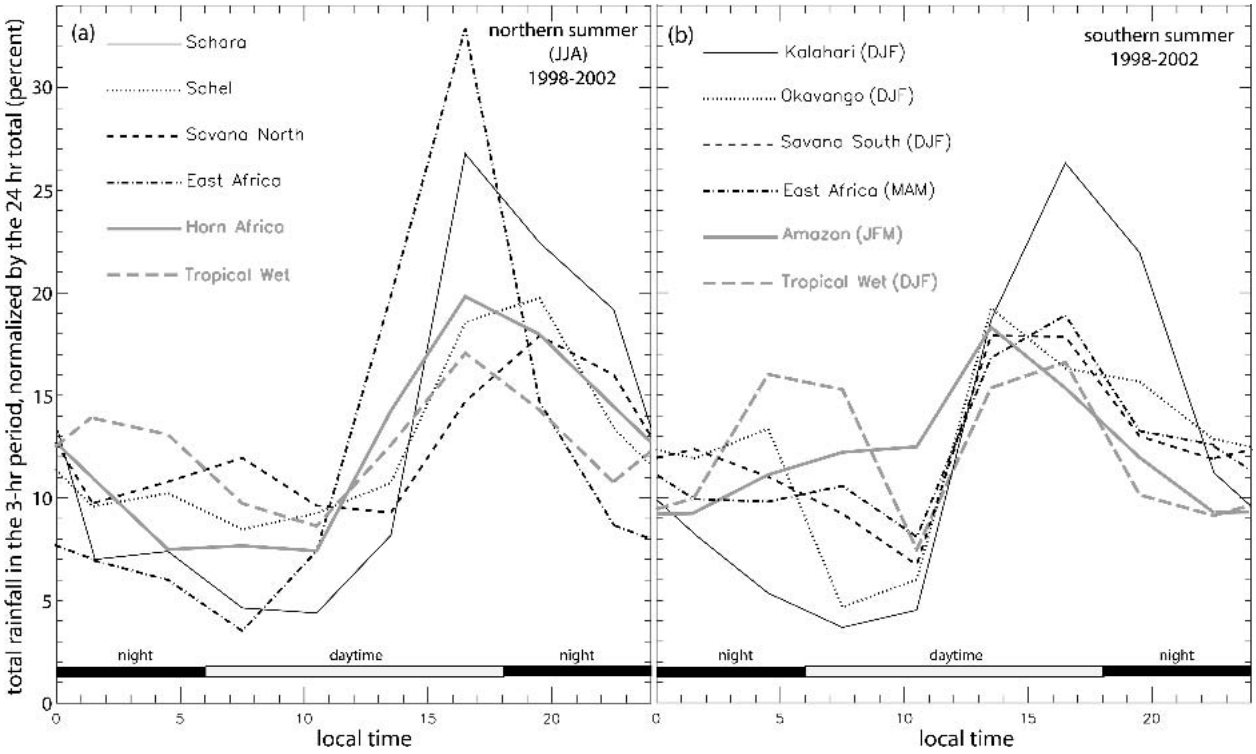

FIG. 10. Diurnal variation of the surface rain total for (a) JJA regions and (b) mostly DJF regions. The total in any 3-h time bin is normalized by the rainfall in all eight time bins, so the average value is 12.5.

the onshore peak seems to occur earlier in the afternoon (1200–1800 LT). As a result, the dawn offshore peak and afternoon onshore peak are separated by only 6 h. Mapes et al. (2003, their Fig. 7) observe a similar asymmetry along the Columbian coastal region, although there some nine hours exist between the dawn offshore and afternoon onshore peaks. The secondary nocturnal peak in the Tropical Wet remains present when the coastal strip is excluded, that is, in the Congo Basin.

b. Storm vertical structure

It was shown in section 3c that the 20-dBZ echo top heights vary regionally. They also vary diurnally, as shown in Fig. 12. On average they are 0.5–2.3 km more shallow in the morning quartile (sunrise to noon) than near sunset in Africa. Mean echo tops generally increase rapidly from just before noon to late afternoon, and then they decrease slowly during the night and early morning. Consistent with the rain-rate variation (Fig. 9), the echo tops in the southern Savanna and Okavango tend to peak earlier in the afternoon (1500–1800 LT) than those in the northern Savanna and Sahel. Also, the diurnal variation of echo top height is weakest in the Amazon, and the Tropical Wet has a secondary maximum before sunrise (at least in DJF). Consistent with Fig. 7, the echo tops tend to be highest in the Sahel and lowest in the Amazon. In East Africa, the diurnal modulations of echo tops, as well as that of rain rate (Fig. 9) and rain amount, are strong in the transition season (JJA), while in the wet season (MAM) they are weaker, and more comparable to that in the Tropical Wet (DJF) region.

We now describe the diurnal variation of the reflectivity FADs as a way to gain an insight into the observed changes in echo top height. Shown in Fig. 13 are the frequencies in any 3-h time bin, normalized as in Fig. 2, and then shown as an anomaly from the 24-h mean, for all echoes observed over five JJA seasons in the Sahel. To clarify, let $N_t(Z, h)$ be the normalized frequency for a reflectivity value Z at a height h, within the time bin t, such that $\Sigma_Z\Sigma_h N_t(Z, h) = 100$. Shown in Fig. 13 is the difference $N_t(Z, h) - \overline{N}(Z, h)$, where $\overline{N}(Z, h)$ is the 24-h mean frequency. Clearly the integrated anomaly, at any time bin, will be zero:

$$\sum_Z \sum_h \{N_t(Z, h) - \overline{N}(Z, h)\} = \sum_Z \sum_h N_t(Z, h) - \sum_Z \sum_h \overline{N}(Z, h) = 100 - 100 = 0. \quad (4)$$

Thus the diurnal anomaly FADs do not reveal the changes in rainfall frequency during the day (shown in

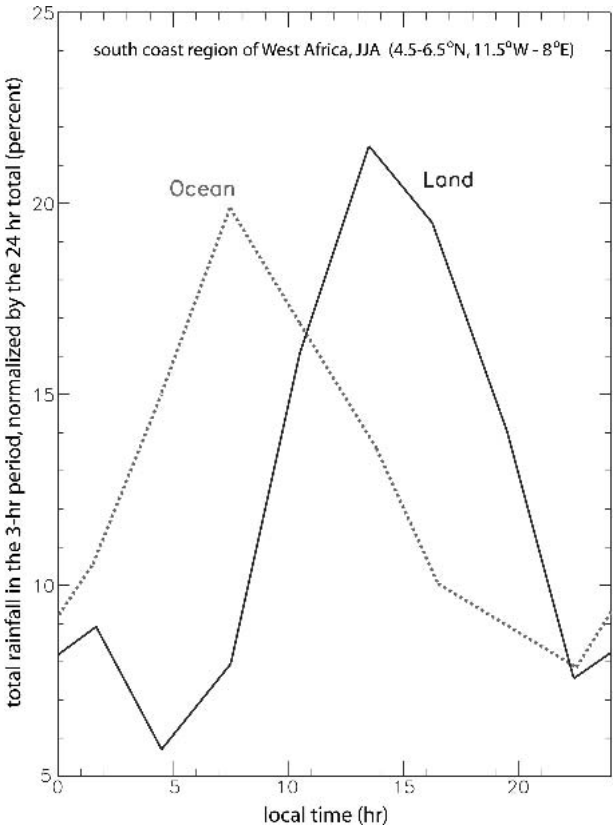

FIG. 11. As in Fig. 10, but for the coastal strip of West Africa in JJA. The land section is contrasted against the coastal Atlantic Ocean.

Fig. 10). They show the anomalous vertical structure of a storm occurring at a certain time, as compared to the normal (daily mean) vertical structure. But for each time bin in Fig. 13, the sample size is shown. The diurnal cycles of the vertical structure of storms in other African regions contain similarities with the patterns shown in Fig. 13 for the Sahel. Diurnal anomaly FADs as the one shown in Fig. 13 were analyzed for the six JJA regions and the six (mainly) DJF regions. The analysis is summarized in Table 4.

Three observations can be drawn from Fig. 13 and Table 4. First, a range of reflectivity values, especially high ones, commonly occur around the FL between 0300–1200 LT. This suggests more frequent stratiform precipitation in that time period. Such "BB max" period does not occur in East Africa (JJA), possibly indicating less storm organization.

Second, echoes below the FL are anomalously common when the sun is high in the sky (0900–1500 LT), suggesting that shallow convection (possibly warm-rain cumuli) are relatively more frequent at that time. This anomaly is more marked in the southern regions than their northern counterparts, and it is especially marked in East Africa, in the JJA transition season. However the latter anomaly occurs remarkably early: it peaks between near dawn (0600–0900 LT; Table 4) in fact it is present between 0000–1200 LT. Echo tops tend to be most shallow in East Africa (JJA) at dawn (Fig. 12), and precipitation light (Fig. 9). Thus we interpret this 0600–0900 LT shallow anomaly as a result of the virtual absence of deep convection over East Africa (JJA) near dawn. This stands in contrast with the Tropical Wet (DJF) region, which also has a nocturnal maximum of shallow events (Table 4), but these events are associated with heavy rain (Figs. 9, 10).

And third, strong, deep echoes prevail in the evening hours (1500–2400 and mainly 1800–2100 LT). This indicates that deep, vigorous convection dominates at that time. The height of this anomaly decreases from the 1500–1800 LT bin to the 2100–2400 LT bin (Fig. 13). This is especially clear in the Sahel, over a large height range, and stronger in the northern (semi)arid regions than in the southern ones.

We summarize the diurnal variation of storm vertical structure in Fig. 14, a FAD of detectable echoes at various times of the day. This diagram reveals changes both in storm vertical structure and in storm frequency. The diurnal amplitude is small in the Tropical Wet and the Amazon, which is consistent with rainfall data (Figs. 9, 10). In other regions, especially the (semi)arid regions and in the transition season (East Africa JJA), storm echoes become more numerous and deeper from 0900–1500 to 1500–2100 LT. Clearly this pulsating echo structure implies diurnal pulses of latent heat release over the African troposphere. Also note that the echo count decays more rapidly with height above the FL at 0300–0900 than at 1500–2100 LT, particularly in the Sahel and northern Savanna regions. This suggests that vigorous convection is less likely around dawn than around sunset, and that storms are more stratiform and less deep around dawn.

5. Discussion

We now aim to interpret the main observations arising from the 2A25 data analysis by means of differences in the large-scale basic-state atmosphere, as documented by the NCEP–NCAR reanalysis dataset. Summarizing the observations, we found that in all regions in Africa, including the Tropical Wet, storms appear more vigorous than over the Amazon. Storms over the Amazon tend to be shallower (Fig. 7; many of them "shallow" or "warm-rain" echoes; Table 2), and they tend to have a lower HPW (Fig. 6), and a better-defined bright-band signature (Fig. 5). Also, reflectivity decays rapidly above the FL in the Amazon region (Fig. 3, Table 3), and the echo strength tends to increase from 4 km toward the ground (Table 3). Within Africa, the Sahel, and to a lesser degree the northern Savanna, stand out for vigorous storms, characterized by high echo tops (Fig. 7) and high hydrometeor loading aloft (Fig. 6). The lack of clear brightband spike (Fig. 2)

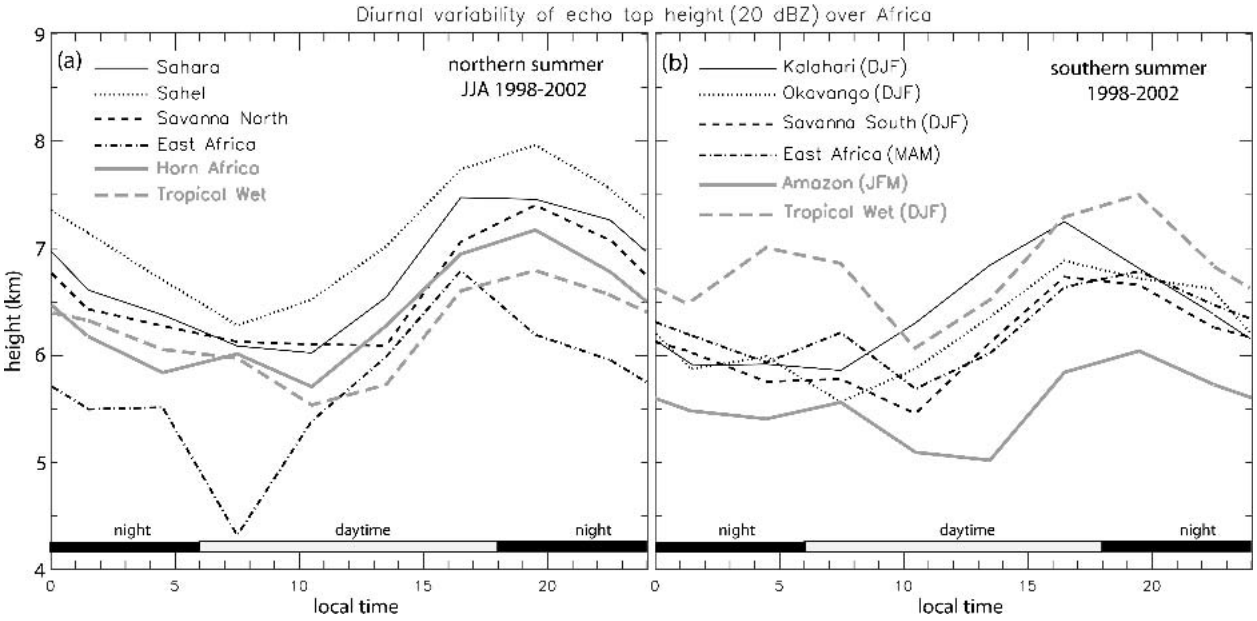

FIG. 12. Diurnal variation of the average 20-dBZ echo top height for (a) JJA regions and (b) mostly DJF regions.

suggests that these storms are mostly convective. In the Sahel and especially the Sahara, there is evidence for low-level evaporation (Table 3). Finally, rainfall (Figs. 9, 10) and vertical storm structure are least diurnally modulated over the Amazon and most strongly in the arid regions of Africa (Fig. 14, Table 4). In many regions the echo tops are highest (Fig. 12) and rainfall most intense (Figs. 9, 10) in afternoon (1500–1800 LT), but the diurnal peak is delayed to 1800–2100 LT in the Sahel and the northern Savanna.

The higher EI and virga fractions in the northern (semi)arid regions (JJA), compared to those south of the equator (DJF; Tables 2, 3), are consistent with the lower climatological relative humidity at the surface in the northern (semi)arid regions (Fig. 15). The average surface relative humidity values are 19%, 51%, and 83% for the Sahara, Sahel, and northern Savanna, respectively (JJA), while they are 37%, 67%, and 83% for the Kalahari, Okavango, and southern Savanna regions, respectively (DJF), according to the NCEP–NCAR reanalysis dataset.

Storm intensity is broadly related to the amount of potential (static) energy harbored in the environment. Shown in Fig. 16 are the profiles of θ_e^* (saturated equivalent potential temperature) for select regions, based on the NCEP–NCAR reanalysis dataset for the corresponding seasons. The reanalysis data are averaged over each region, except for the Sahara where only the southern third is used (15°–20°N), because almost all of the storms in the Sahara database (Table 1) occurred there. From the θ_e^* profile and the equivalent potential temperature θ_e at 1000 mb ($\theta_{e,\mathrm{sfc}}$), one can estimate the level of free convection (LFC$_e$, mb) as the level where the $\theta_{e,\mathrm{sfc}}$ value intersects the ambient θ_e^* curve. This LFC$_e$ is not the same as the LFC traditionally defined on an aerological diagram, but it is related. The reason is that the θ_e of an undiluted parcel rising from the surface is conserved, thus above the LFC$_e$, where the parcel is saturated, the parcel θ_e (or moist static energy) is larger than the ambient θ_e^* and thus also the ambient θ_e.

We also compute a measure of convective available potential energy (CAPE; J kg^{-1}). The CAPE is the integral of the buoyancy of an undiluted parcel from the LFC to the level of neutral buoyancy (LNB). We define the latter as the level where $\theta_{e,\mathrm{sfc}}$ rejoins the ambient θ_e^* curve (Fig. 16), and denote it as LNB$_e$. We then define a measure of CAPE (CAPE$_e$) as the excess of $\theta_{e,\mathrm{sfc}}$ over the ambient θ_e^*, following Petersen and Rutledge (2001) and others. Thus

$$\mathrm{CAPE}_e = R_d \int_{\mathrm{LFC}_e}^{\mathrm{LNB}_e} (\theta_e^* - \theta_{e,\mathrm{sfc}}) d \ln p, \qquad (5)$$

where R_d is the specific gas constant for dry air (287 J kg^{-1} K^{-1}). The derivation of CAPE$_e$, LFC$_e$, and LNB$_e$ is shown in Fig. 16, and their values are listed in Table 5. The CAPE$_e$ values are larger than the true CAPE values in the vicinity of storms, which may be surprising since that CAPE based on climatological values normally is much less than the preconvective CAPE. Clearly CAPE and CAPE$_e$ are not the same, and the purpose here is merely to compare CAPE$_e$ values between regions. The highest CAPE$_e$ value is found in the Sahel, followed by the Tropical Wet (DJF; Table 5). These CAPE$_e$ values are more than twice that in the Amazon. The difference is due less to differences in the θ_e^* profiles, but rather to the higher value of $\theta_{e,\mathrm{sfc}}$

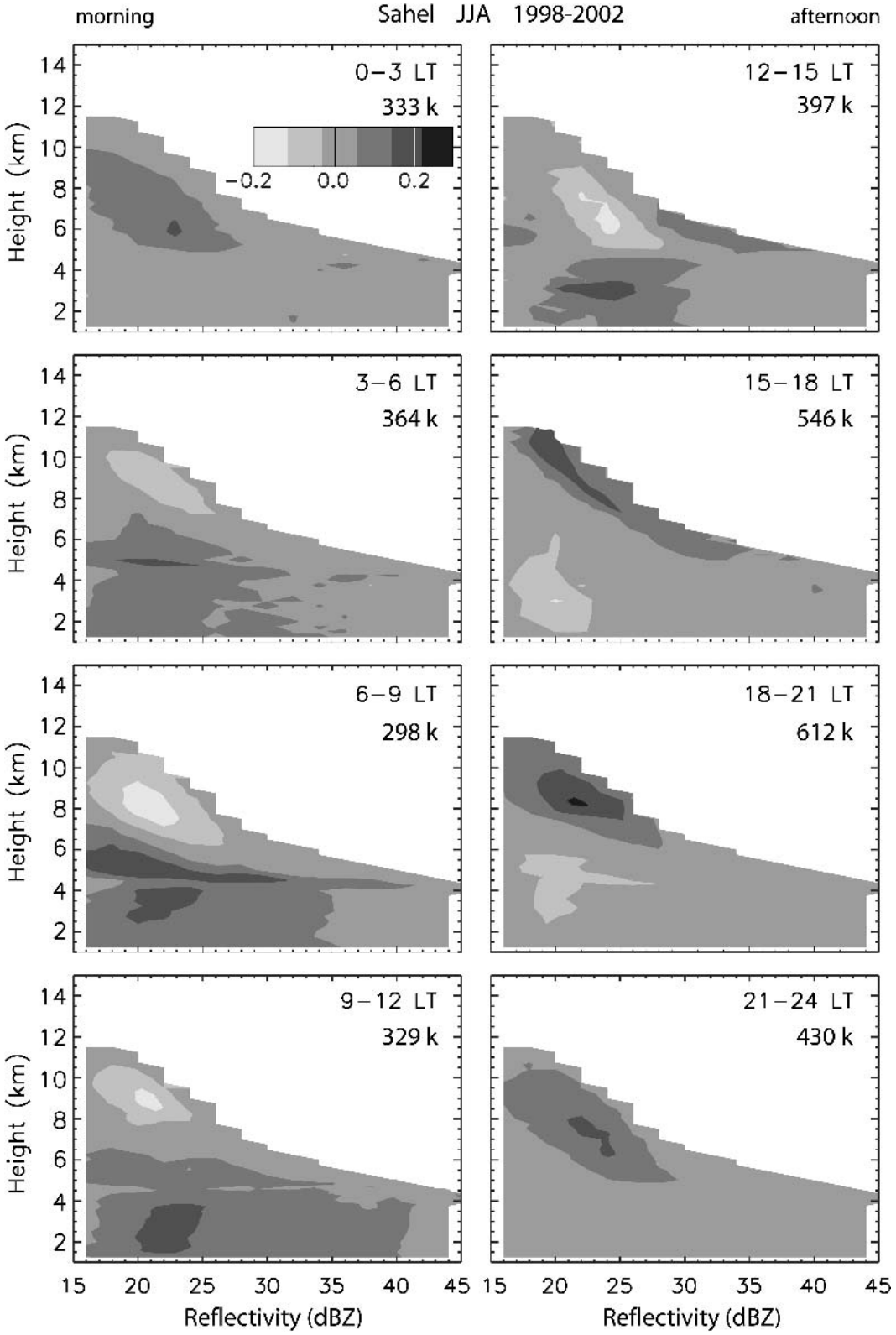

FIG. 13. Diurnal variation of the reflectivity FAD, for the Sahel [units $(2\ \mathrm{dB}Z)^{-1}\ (250\ \mathrm{m})^{-1}$]. The normalized frequencies are expressed as a difference from the normalized 24-h mean values. The total number of occurrences in a time bin is shown for each FAD.

TABLE 4. Summary of the diurnal variations of the reflectivity FAD in various regions. The figures are derived from FADs as the ones in Fig. 13, for each region. The "strength" is the peak strength of the positive anomaly, in normalized units as displayed in Fig. 13. The "period" refers to the local time during which this anomaly occurred (3-h bins). The "height" is the level of the peak strength of the positive anomaly. The "BB max" column lists the time period when echoes of various strengths are anomalously frequent at the freezing level.

		Shallow maxima			Deep maxima			BB max
Region	Season (units)	Period (h LT)	Height (km)	Strength 1/(2 dBZ)(250 m)	Period (h LT)	Height (km)	Strength 1/(2 dBZ)(250 m)	Period (h LT)
Sahara	JJA	1200–1500	4.0	0.19	1800–2400	7.75	0.25	0600–1200
Sahel	JJA	0900–1500	3.0	0.21	1500–2400	8.5	0.29	0300–0900
Savanna North	JJA	1200–1500	2.5	0.17	1800–2400	8.5	0.21	0300–1200
Tropical Wet	JJA	0900–1500	2.25	0.27	1800–2400	7.5	0.20	0300–0900
East Africa	JJA	0600–0900	2.25	0.43	1800–2400	8.0	0.19	—
Horn Africa	JJA	0900–1200	3.75	0.30	1800–2400	8.5	0.29	0300–0600
Kalahari	DJF	0000–0900	2.75–3.5	0.28	1500–2100	7.5	0.23	0600–0900
Okavango	DJF	0900–1200	2.75	0.22	1500–2400	7.75	0.20	0300–0900
Savanna South	DJF	0900–1200	3	0.26	1500–2100	8.0	0.29	0000–0900
Tropical Wet	DJF	0000–0300	3.25	0.22	1500–2100	9.0	0.19	0900–1200
		1200–1500	3	0.17				
East Africa	MAM	0900–1200	2.25	0.20	1800–2400	7.75	0.19	0300–0600
Amazon	JFM	0900–1500	2–2.75	0.14	1500–2100	8.25	0.16	0600–0900

in the Sahel (and the Tropical Wet), compared to the Amazon. The higher $\theta_{e,\mathrm{sfc}}$ in the Sahel is mostly due to a higher temperature there (5–7 K), not a higher relative humidity, compared to the Amazon. The Sahel and Tropical Wet (DJF) regions also have a more elevated LNB_e than does the Amazon (Table 5), which is consistent with the more frequent occurrence of PR-measurable echoes at upper levels in those regions (Fig. 7). In a broader context, our findings are consistent with several TRMM-based studies that indicate that the most intense storms in the Earth's tropical belt (23.5°N–23.5°S) are found in Africa [see review article by Zipser (2003)]. The relatively weaker, more stratiform storms and higher warm-rain fraction over the Amazon are consistent with the lower CAPE and lower LFC there, compared to wet-season values anywhere in tropical Africa. The fundamental reason for this difference is that trade winds from the Indian Ocean are partially blocked by the high terrain of eastern Africa, while in the Amazon the blocking high terrain is on the downwind west side of the basin.

The Sahara has the lowest CAPE_e in Table 5, which is due to the low specific humidity there: $\theta^*_{e,\mathrm{sfc}}$ greatly exceeds $\theta_{e,\mathrm{sfc}}$ (Fig. 16). As a consequence the LFC_e is nearly 1 km higher than in the other regions. The θ^*_e continues to be higher in the Sahara than in other regions up to about 500 mb, mainly because of higher temperatures, but in the upper troposphere θ^*_e is slightly lower than in most other regions, which is consistent with the rather high echo tops of Sahara storms (Fig. 7). In fact, the secondary echo top maximum around 6–7 km (Fig. 7) may be related to the deeper layer of conditional instability ($\theta^*_e/p > 0$) in the Sahara, compared to that in other regions (Fig. 16).

Finally we interpret the diurnal delay in rainfall and echo top height maxima in the Sahel and the northern Savanna, compared to other regions in Africa. This delay may be related to land cover (Mohr et al. 2003), but it is more likely that deep convection, triggered by daytime heating, becomes more organized during the evening. This is consistent with the larger low-level wind shear there, which is a factor in the longevity of squall lines (Rotunno et al. 1988). In JJA, the climatological wind shear in the lowest 3 km (1000–700 mb) is northeasterly and its magnitude averages (peaks) at $3.7\ 10^{-3}$ s^{-1} ($5.0\ 10^{-3}\ \mathrm{s}^{-1}$) in the Sahel and northern Savanna, according to the NCEP–NCAR reanalysis dataset. The climatological DJF wind shear for the Okavango and southern Savanna regions over roughly the same depth (between the level closest to the ground, 850 and 550 mb) is mostly southeasterly and its magnitude averages (peaks) at merely $1.2\ 10^{-3}\ \mathrm{s}^{-1}$ ($1.7\ 10^{-3}\ \mathrm{s}^{-1}$). Under weak shear, short-lived airmass thunderstorms prevail, and these are most numerous earlier in the afternoon. According to numerical simulations by Weisman et al. (1988), the optimal shear for long-lived squall lines is 15–25 $\mathrm{m\ s}^{-1}$ over the lowest 2.5 km. Several long-lived squall lines have been documented in the northern Savanna region (e.g., Roux et al. 1984), and IR satellite imagery suggests that large organized convective systems are far more common in the northern zenithal rain belt than in the southern one (Laing and Fritsch 1993). The weak diurnal cycle of rain rate in the northern Savanna (Fig. 9) and the secondary maximum in rain amount near dawn (Fig. 10: 0600–0900 LT in the northern Savanna; 0300–0600 LT in the Sahel and even the Sahara) is consistent with the eastward progression of nocturnal squall lines across the subSaharan zenithal rain belt in JJA, which has been observed on several occasions in the western Sahel (Chalon et al. 1988; Roux and Sun 1990). This is not unlike the nocturnal westward progression of organized convection across the Plains of the central United States (Carbone et al. 2002).

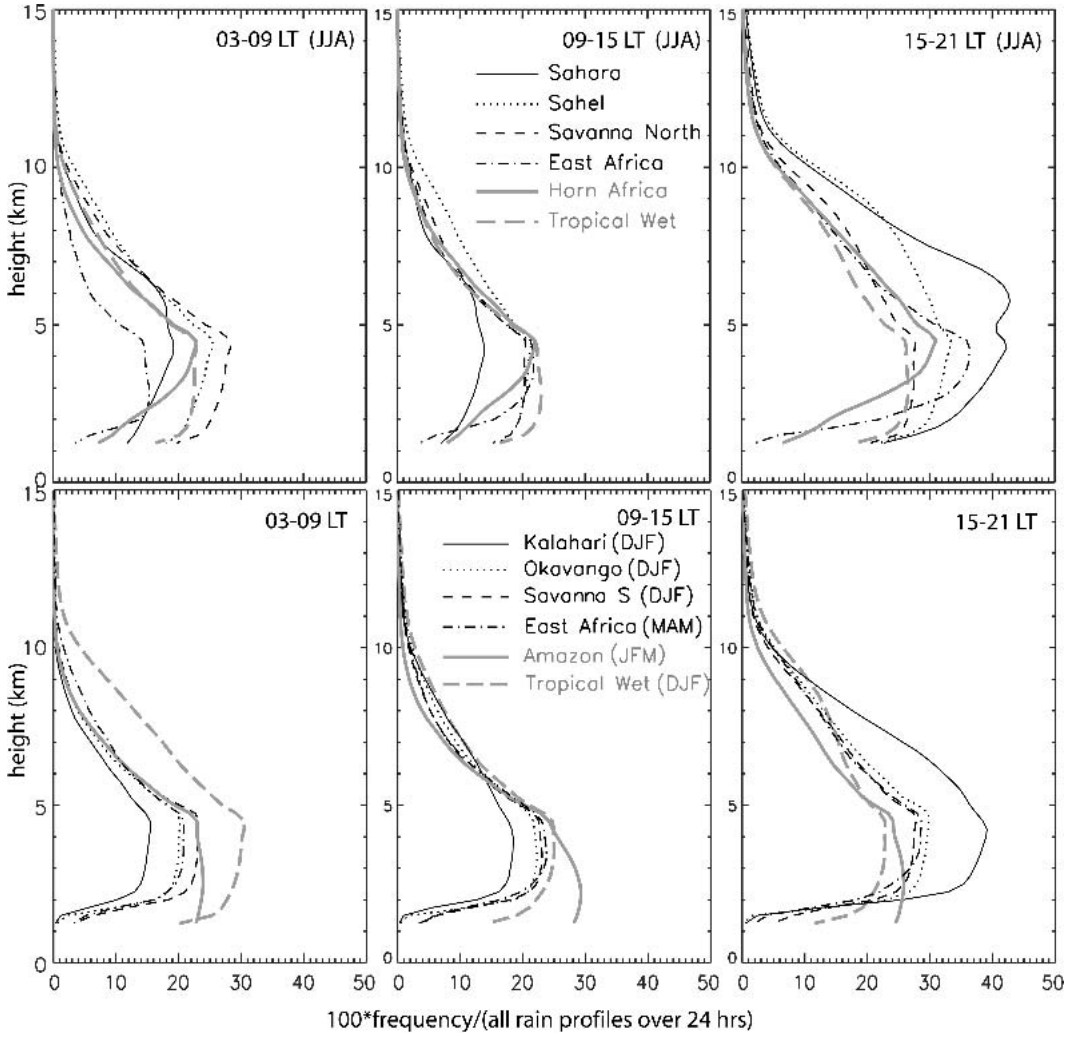

FIG. 14. As Fig. 5, but for one threshold only (17 dBZ). Three 6-h periods are isolated: (left) 0300–0900, (middle) 0900–1500, and (right) 1500–2100 LT. Frequencies are normalized by the total number of rain profiles in each region. (top) JJA regions and (bottom) DJF regions. Note that all x axes are the same.

6. Conclusions

This study aims to describe the regional and diurnal variability of the vertical structure of storms in tropical Africa, by means of 5 yr of extreme-season (DJF and JJA) TRMM Precipitation Radar data. The regional storm characteristics are contrasted against those in the Amazon. The key TRMM product used here is the 2A25 reflectivity profile, which is truncated at about 17 dBZ, and the radar-derived surface rain rate. The main findings of this study are as follows.

- In all of tropical Africa, including the Tropical Wet region (which is mainly the Congo Basin), storms tend to be more vigorous than over the Amazon. Storms over the Amazon tend to be more shallow, and warm-rain events (whose echoes peak below the freezing level) are more common. Amazon storms are less likely to have high reflectivity values aloft, and they have a better-defined brightband signature.
- Some regional differences in storm vertical structure exists within tropical Africa, although these are small compared to that between the Amazon and Africa. Vigorous storms frequent the Sahel, and to a lesser degree the adjacent northern Savanna and the Tropical Wet region (in the latter especially in DJF). Sahel storms are marked by high echo tops and high hydrometeor loading aloft. The lack of a clear brightband spike suggests that these storms are mostly convective. Comparing the northern (semi)arid regions (the Sahel and the Sahara) to the southern ones (the Okavango and Kalahari, respectively), low-level evaporation is more common/intense in the former

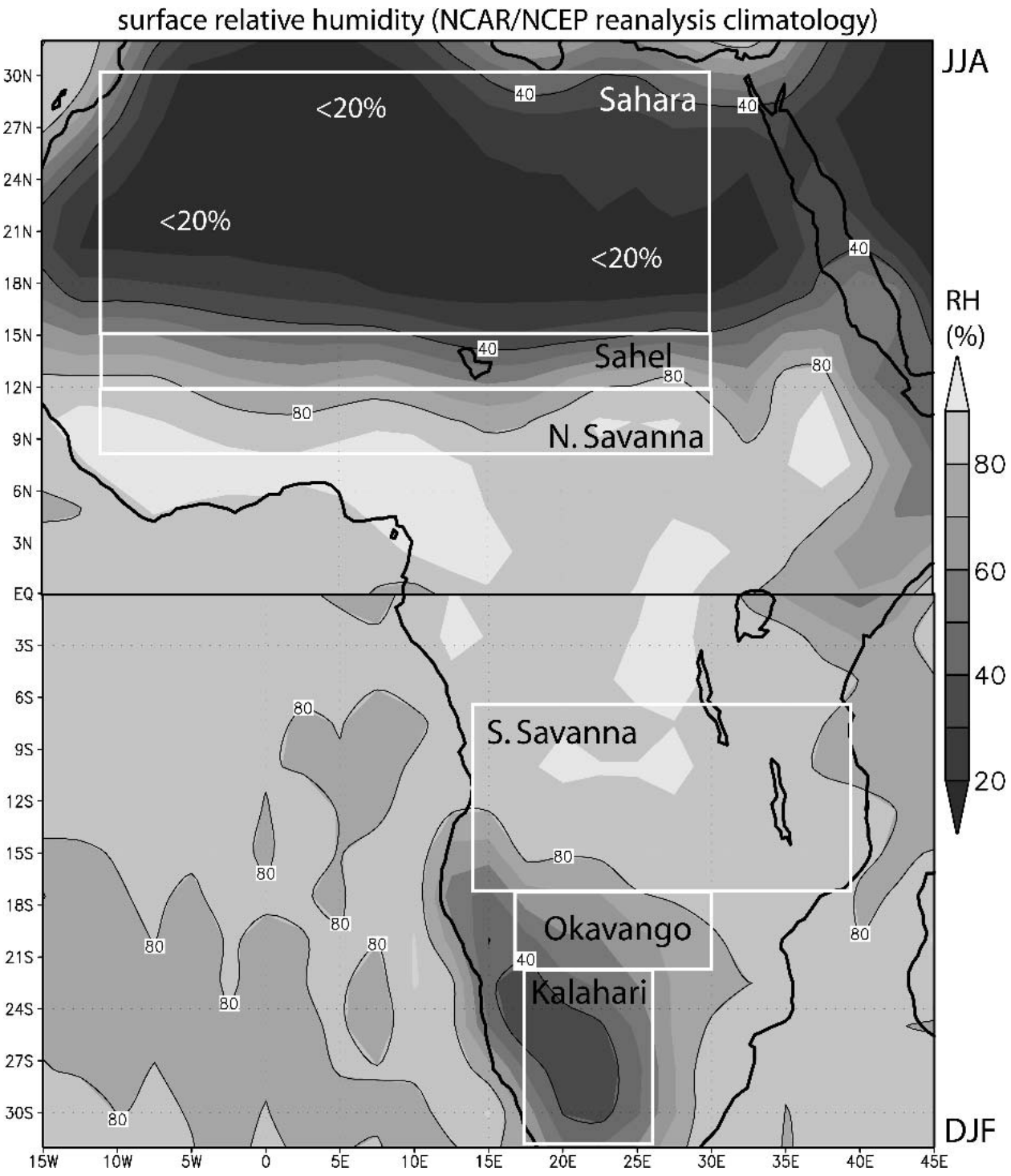

FIG. 15. The climatological surface relative humidity, according to the NCEP–NCAR reanalysis dataset for JJA (north of the equator) and DJF (south of the equator).

regions and warm-rain events are more common in the latter.

- The diurnal modulation of rainfall and vertical storm structure is minimal over the Amazon and largest in the arid regions of Africa. In many African regions the echo tops are highest and rainfall is most intense in the afternoon (1500–1800 local time), but the diurnal peak is delayed by a few hours in the Sahel and

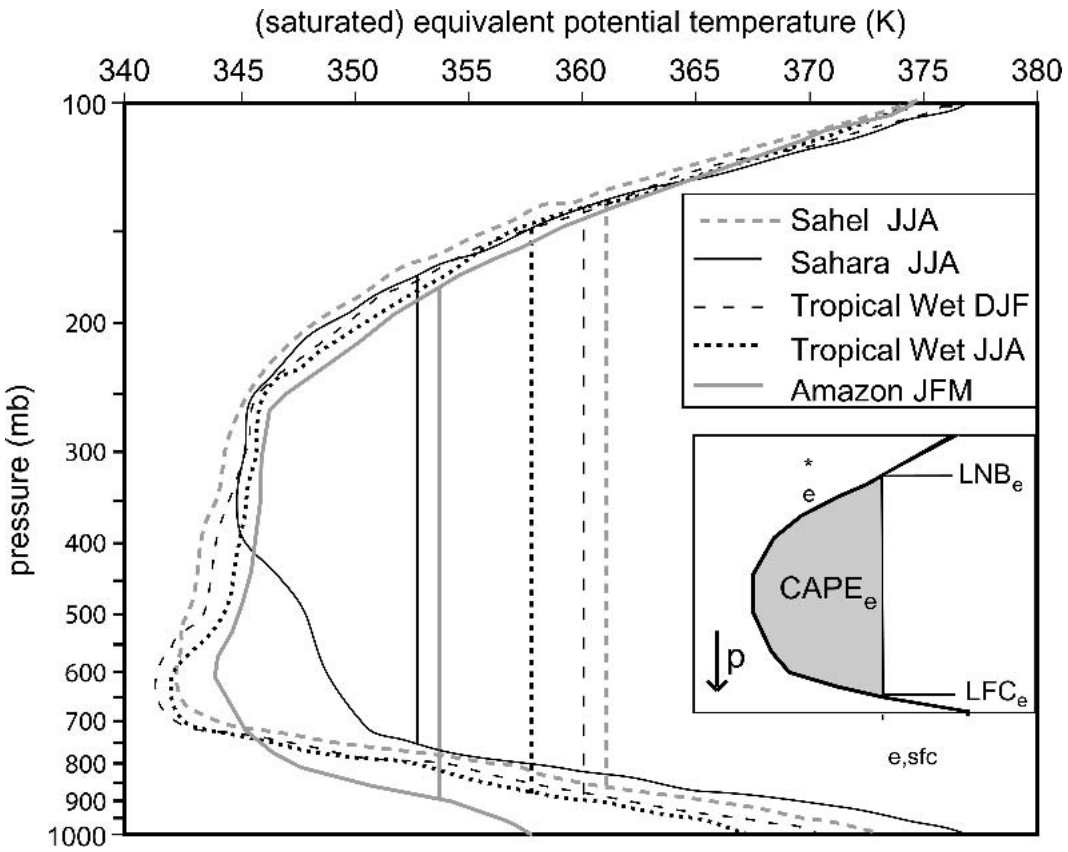

FIG. 16. Vertical profiles of θ_e^* (curved lines) plotted as a function of pressure (log coordinates, i.e., height) for various regions. The vertical lines are corresponding values of surface θ_e, derived from the temperature and the specific humidity at 1000 mb. Data are based on the NCEP–NCAR reanalysis dataset. These data are averaged over the full area of each region except for the Sahara, where only the southern third (15°–20°N) is used.

the northern Savanna. The echo top height and rainfall distribution in the Tropical Wet region has a secondary maximum in the second half of the night.

- The regional variation of the vertical structure of storms in Africa, and the contrast between Africa and the Amazon, are consistent with thermodynamic properties of the basic-state environment.

This study has focused on the typical vertical structure of storms in Africa. In a follow-up study, we plan to examine interannual variability of precipitation systems in Africa, in the context of observed departures from the mean flow and thermodynamic conditions.

TABLE 5. Values of CAPE$_e$, LFC$_e$, and LNB$_e$ inferred from the profiles shown in Fig. 16.

Region	Season	CAPE$_e$ (J kg^{-1})	LFC$_e$ (mb)	LNB$_e$ (mb)
Sahel	JJA	7375	864	137
Sahara	JJA	2214	758	176
Tropical Wet	DJF	6776	873	141
Tropical Wet	JJA	5427	876	149
Amazon	JFM	3059	886	185

Acknowledgments. This research was supported by the National Aeronautics and Space Administration EPSCoR Grant 5-33395. The second author benefited from the interaction with Mircea Grecu, Erich Stocker, and others at NASA Goddard Code 912 during and after his Earth Science Enterprise summer 2003 graduate fellowship.

REFERENCES

Adeyewa, Z. D., and K. Nakamura, 2003: Validation of TRMM radar rainfall data over major climatic regions in Africa. *J. Appl. Meteor.,* **42,** 331–347.

Anagnostou, E. N., C. A. Morales, and T. Dinku, 2001: The use of TRMM precipitation radar observations in determining ground radar calibration biases. *J. Atmos. Oceanic Technol.,* **18,** 616–628.

Battan, L. J., 1973: *Radar Observations of the Atmosphere*. University of Chicago Press, 324 pp.

Bell, T. L., and N. Reid, 1993: Detecting the diurnal cycle of rainfall using satellite observations. *J. Appl. Meteor.,* **32,** 311–322.

Berg, W., C. Kummerow, and C. A. Morales, 2002: Differences between east and west Pacific rainfall systems. *J. Climate,* **15,** 3659–3672.

Boccippio, D. J., S. J. Goodman, and S. Heckman, 2000: Regional

differences in tropical lightning distributions. *J. Appl. Meteor.,* **39,** 2231–2248.

Carbone, R. E., J. D. Tuttle, D. A. Ahijevych, and S. B. Trier, 2002: Inferences of predictability associated with warm season precipitation episodes. *J. Atmos. Sci.,* **59,** 2033–2056.

Cecil, D. J., and E. J. Zipser, 2002: Reflectivity, ice scattering, and lightning characteristics of hurricane eyewalls and rainbands. Part II: Intercomparison of observations. *Mon. Wea. Rev.,* **130,** 785–801.

Chalon, J. P., G. Jaubert, J. P. Lafore, and F. Roux, 1988: The West African squall line observed on 23 June 1981 during COPT 81: Mesoscale structure and transports. *J. Atmos. Sci.,* **45,** 2744–2763.

Dai, A., 2001: Global precipitation and thunderstorm frequencies. Part II: Diurnal variations. *J. Climate,* **14,** 1112–1128.

——, F. Giorgi, and K. E. Trenberth, 1999: Observed and model simulated precipitation diurnal cycle over the contiguous United States. *J. Geophys. Res.,* **104,** 6377–6402.

Davis, C. A., K. W. Manning, R. E. Carbone, S. B. Trier, and J. D. Tuttle, 2003: Coherence of warm-season continental rainfall in numerical weather prediction models. *Mon. Wea. Rev.,* **131,** 2667–2679.

Durden, S. L., Z. S. Haddad, A. Kitiyakara, and F. K. Li, 1998: Effects of non-uniform beam filling on rainfall retrieval for the TRMM precipitation radar. *J. Atmos. Oceanic Technol.,* **15,** 635–646.

Ferreira, F., P. Amayenc, S. Oury, and J. Testud, 2001: Study and tests of improved rain estimates from the TRMM precipitation radar. *J. Appl. Meteor.,* **40,** 1878–1899.

Fisher, B. L., 2004: Climatological validation of TRMM TMI and PR monthly rain products over Oklahoma. *J. Appl. Meteor.,* **43,** 519–535.

Geerts, B., and Y. Dawei, 2004a: Classification and characterization of tropical precipitation based on high-resolution airborne vertical-incidence radar. Part I: Classification. *J. Appl. Meteor.,* **43**, 1554–1566.

——, and ——, 2004b: Classification and characterization of tropical precipitation based on high-resolution airborne vertical incidence radar. Part II: Composite vertical structure of hurricanes versus storms over Florida and the Amazon. *J. Appl. Meteor.,* **43**, 1567–1585.

Heymsfield, G. M., B. Geerts, and L. Tian, 2000: TRMM precipitation radar reflectivity profiles as compared with high-resolution airborne and ground-based radar measurements. *J. Appl. Meteor.,* **39,** 2080–2102.

Hirose, M., and K. Nakamura, 2002: Spatial and seasonal variation of rain profiles over Asia observed by space-borne precipitation radar. *J. Climate,* **15,** 3443–3458.

Hobbs, P. V., T. J. Matejka, P. H. Herzegh, J. D. Locatelli, and R. A. Houze, 1980: The mesoscale and microscale structure and organization of clouds and precipitation in midlatitude cyclones. Part I: A case study of a cold front. *J. Atmos. Sci.,* **37,** 568–596.

Houze, R. A., Jr., 1993: *Cloud Dynamics*. Academic Press, 573 pp.

——, 1997: Stratiform precipitation in regions of convection: A meteorological paradox? *Bull. Amer. Meteor. Soc.,* **78,** 2179–2196.

——, S. G. Geotis, F. D. Marks Jr., and A. K. West, 1981: Winter monsoon convection in the vicinity of north Borneo. Part I: Structure and time variation of the clouds and precipitation. *Mon. Wea. Rev.,* **109,** 1595–1614.

Huffman, G. J., and Coauthors, 1997: The Global Precipitation Climatology Project (GPCP) combined precipitation dataset. *Bull. Amer. Meteor. Soc.,* **78,** 5–20.

Iguchi, T., and R. Meneghini, 1994: Intercomparison of single-frequency methods for retrieving a vertical rain profile from airborne or spaceborne radar data. *J. Atmos. Oceanic Technol.,* **11,** 1507–1516.

——, T. Kozu, R. Meneghini, J. Awaka, and K. Okamoto, 2000: Rain-profiling algorithm for the TRMM precipitation radar. *J. Appl. Meteor.,* **39,** 2038–2052.

Jensen, M. P., and A. D. Del Genio, 2003: Radiative and microphysical characteristics of deep convective systems in the tropical western Pacific. *J. Appl. Meteor.,* **42,** 1234–1254.

Johnson, R. H., T. M. Rickenbach, S. A. Rutledge, P. E. Ciesielski, and W. H. Schubert, 1999: Trimodal characteristics of tropical convection. *J. Climate,* **12,** 2397–2418.

Kalnay, E., and Coauthors, 1996: The NCAR/NCEP 40-Year Reanalysis Project. *Bull. Amer. Meteor. Soc.,* **77,** 437–471.

Kummerow, C., and L. Giglio, 1994: A passive microwave technique for estimating rainfall and vertical structure information from space. Part I: Algorithm description. *J. Appl. Meteor.,* **33,** 3–18.

——, W. Barnes, T. Kozu, J. Shiue, and J. Simpson, 1998: The Tropical Rainfall Measuring Mission (TRMM) sensor package. *J. Atmos. Oceanic Technol.,* **15,** 809–817.

——, and Coauthors, 2000: The status of the Tropical Rainfall Measuring Mission (TRMM) after two years in orbit. *J. Appl. Meteor.,* **39,** 1965–1982.

Laing, A. G., and J. M. Fritsch, 1993: Mesoscale convective complexes in Africa. *Mon. Wea. Rev.,* **121,** 2254–2263.

Lebel, T., and A. Amani, 1999: Rainfall estimation in the Sahel: What is the ground truth? *J. Appl. Meteor.,* **38,** 555–568.

Leroux, M., 2001: *The Meteorology and Climate of Tropical Africa*. Springer-Verlag, 548 pp.

Lin, X., D. A. Randall, and L. D. Fowler, 2000: Diurnal variability of the hydrologic cycle and radiative fluxes: Comparisons between observations and a GCM. *J. Climate,* **13,** 4159–4179.

Mapes, B. E., and R. A. Houze, 1993: Cloud clusters and superclusters over the oceanic warm pool. *Mon. Wea. Rev.,* **121,** 1398–1416.

——, T. T. Warner, M. Xu, and A. J. Negri, 2003: Diurnal patterns of rainfall in northwestern South American. Part I: Observations and context. *Mon. Wea. Rev.,* **131,** 799–812.

Masunaga, H., T. Iguchi, R. Oki, and M. Kachi, 2002: Comparison of rainfall products derived from TRMM Microwave Imager and Precipitation Radar. *J. Appl. Meteor.,* **41,** 849–862.

Mohr, K. I., D. R. Baker, W.-K. Tao, and J. S. Famiglietti, 2003: The sensitivity of West African convective line water budgets to land cover. *J. Hydrometeor.,* **4,** 62–76.

Negri, A. J., R. F. Adler, E. J. Nelkin, and G. J. Huffman, 1994: Regional rainfall climatologies derived from Special Sensor Microwave Imager (SSM/I) data. *Bull. Amer. Meteor. Soc.,* **75,** 1165–1182.

——, T. L. Bell, and L. Xu, 2002: Sampling of the diurnal cycle of precipitation using TRMM. *J. Atmos. Oceanic Technol.,* **19,** 1333–1344.

Nesbitt, S. W., and E. J. Zipser, 2003: The diurnal cycle of rainfall and convective intensity according to three years of TRMM measurements. *J. Climate,* **16,** 1456–1475.

Nicholson, S. E., B. Some, and B. Kone, 2000: An analysis of recent rainfall conditions in West Africa, including the rainy seasons of the 1997 El Niño and the 1998 La Niña years. *J. Climate,* **13,** 2628–2640.

——, and Coauthors, 2003: Validation of TRMM and other rainfall estimates with a high-density gauge dataset for West Africa. Part II: Validation of TRMM rainfall products. *J. Appl. Meteor.,* **42,** 1355–1368.

Petersen, W. A., and S. A. Rutledge, 2001: Regional variability in tropical convection: Observations from TRMM. *J. Climate,* **14,** 3566–3586.

——, S. W. Nesbitt, R. J. Blakeslee, R. Cifelli, P. Hein, and S. A. Rutledge, 2002: TRMM observations of intraseasonal variability in convective regimes over the Amazon. *J. Climate,* **15,** 1278–1294.

Petty, G. W., 1999: Prevalence of precipitation from warm-topped clouds over eastern Asia and the western Pacific. *J. Climate,* **12,** 220–229.

Rickenbach, T. M., 2004: Nocturnal cloud systems and the diurnal

variation of clouds and rainfall in southwestern Amazonia. *Mon. Wea. Rev.,* **132,** 1201–1219.

Roux, F., and J. Sun, 1990: Single-Doppler observations of a West African squall line on 27–28 May 1981 during COPT 81: Kinematics, thermodynamics, and water budget. *Mon. Wea. Rev.,* **118,** 1826–1854.

——, J. Testud, M. Payen, and B. Pinty, 1984: West African squall-line thermodynamic structure retrieved from dual-Doppler radar observations. *J. Atmos. Sci.,* **41,** 3104–3121.

Rotunno, R., J. B. Klemp, and M. L. Weisman, 1988: A theory for strong, long-lived squall lines. *J. Atmos. Sci.,* **45,** 463–485.

Sauvageot, H., F. Mesnard, and R. S. Tenorio, 1999: The relation between the area-average rain rate and the rain cell size distribution parameters. *J. Atmos. Sci.,* **56,** 57–70.

Short, D. A., and K. Nakamura, 2000: TRMM radar observations of shallow precipitation over the tropical oceans. *J. Climate,* **13,** 4107–4124.

Smull, B. F., and R. A. Houze, 1987: Rear inflow in squall lines with trailing stratiform precipitation. *Mon. Wea. Rev.,* **115,** 2869–2889.

Sorooshian, S., X. Gao, K. Hsu, R. A. Maddox, Y. Hong, H. V. Gupta, and B. Imam, 2002: Diurnal variability of tropical rainfall retrieved from combined GOES and TRMM satellite information. *J. Climate,* **15,** 983–1001.

Steiner, M., and R. A. Houze Jr., 1997: Sensitivity of the estimated monthly convective rain fraction to the choice of Z–R relation. *J. Appl. Meteor.,* **36,** 452–462.

Stith, J. L., J. E. Dye, A. Bansemer, A. J. Heymsfield, C. A. Grainger, W. A. Petersen, and R. Cifelli, 2002: Microphysical observations of tropical clouds. *J. Appl. Meteor.,* **41,** 97–117.

Toracinta, E. R., D. J. Cecil, E. J. Zipser, and S. W. Nesbitt, 2002: Radar, passive microwave, and lightning characteristics of precipitating systems in the Tropics. *Mon. Wea. Rev.,* **130,** 802–824.

Vicente, G. A., R. A. Scofield, and W. P. Menzel, 1998: The operational GOES infrared rainfall estimation technique. *Bull. Amer. Meteor. Soc.,* **79,** 1883–1898.

Weisman, M. L., J. B. Klemp, and R. Rotunno, 1988: Structure and evolution of numerically simulated squall lines. *J. Atmos. Sci.,* **45,** 1990–2013.

Wilcox, E. M., and V. Ramanathan, 2001: Scale dependence of the thermodynamic forcing of tropical monsoon clouds: Results from TRMM observations. *J. Climate,* **14,** 1511–1524.

Zipser, E. J., 2003: Some views on "hot towers" after 50 years of tropical field programs and two years of TRMM data. *Cloud Systems, Hurricanes, and the Tropical Rainfall Measuring Mission (TRMM): A Tribute to Dr. Joanne Simpson, Meteor. Monogr.,* No. 29, Amer. Meteor. Soc., 49–69.